

# Tropospheric NO<sub>2</sub> vertical profiles over South Korea and their relation to oxidant chemistry: Implications for geostationary satellite retrievals and the observation of NO<sub>2</sub> diurnal variation from space

Laura Hyesung Yang<sup>1</sup>, Daniel J. Jacob<sup>1,2</sup>, Nadia K. Colombi<sup>2</sup>, Shixian Zhai<sup>1</sup>, Kelvin H. Bates<sup>1,3</sup>, Viral Shah<sup>4</sup>, Ellie Beaudry<sup>1</sup>, Robert M. Yantosca<sup>1</sup>, Haipeng Lin<sup>1</sup>, Jared F. Brewer<sup>2</sup>, Heesung Chong<sup>6</sup>, Katherine R. Travis<sup>7</sup>, James H. Crawford<sup>7</sup>, Lok Lamsal<sup>8,9</sup>, Ja-Ho Koo<sup>10</sup>, Jhoon Kim<sup>10</sup>

<sup>1</sup> Harvard University, John A. Paulson School of Engineering and Applied Sciences, Cambridge, MA 02138, USA

<sup>2</sup> Harvard University, Department of Earth and Planetary Sciences, Cambridge, MA 01238, USA

<sup>3</sup> University of California Davis, Department of Environmental Toxicology, Davis CA 95616, USA

10 <sup>4</sup> Global Modeling and Assimilation Office, NASA Goddard Space Flight Center, Greenbelt, MD 20771, USA, and Science Systems and Applications, Inc., Lanham, MD 20706, USA

<sup>5</sup> University of Minnesota, Department of Soil, Water and Climate, St. Paul, Minnesota, USA

<sup>6</sup> Harvard-Smithsonian Center for Astrophysics, Cambridge, Massachusetts 02138, USA

<sup>7</sup> NASA Langley Research Center, Hampton, VA 23666, USA

15 <sup>8</sup> Atmospheric Chemistry and Dynamics Laboratory, NASA Goddard Space Flight Center, Greenbelt, MD 20771, USA

<sup>9</sup> University of Maryland Baltimore County, Baltimore, MD 21250, USA

<sup>10</sup> Yonsei University, Department of Atmospheric Sciences, Seoul, South Korea

Correspondence to: Laura Hyesung Yang ([laurayang@g.harvard.edu](mailto:laurayang@g.harvard.edu))

20 **Abstract.** Nitrogen oxides (NO<sub>x</sub> ≡ NO + NO<sub>2</sub>) are of central importance for air quality, climate forcing, and nitrogen deposition to ecosystems. The Geostationary Environment Monitoring Spectrometer (GEMS) is now providing hourly NO<sub>2</sub> satellite observations over East Asia, offering the first direct measurements of NO<sub>2</sub> diurnal variation from space to guide understanding of NO<sub>x</sub> emissions and chemistry. The NO<sub>2</sub> retrieval requires independent vertical profile information from a chemical transport model (CTM) to compute the air mass factor (AMF) that relates the NO<sub>2</sub> column measured along the line of sight to the NO<sub>2</sub> vertical column. Here, we use aircraft observations from the Korea-United States Air Quality (KORUS-AQ) campaign over the Seoul Metropolitan Area (SMA) and around the Korean peninsula in May-June 2016 to better understand the factors controlling the NO<sub>2</sub> vertical profile, its diurnal variation, the implications for the AMF, and the ability of the GEOS-Chem CTM to compute the NO<sub>2</sub> vertical profiles used for AMF. Proper representation of oxidant chemistry is critical for the CTM simulation of NO<sub>2</sub> vertical profiles and is achieved in GEOS-Chem through new model developments including aerosol nitrate photolysis, reduced uptake of hydroperoxy (HO<sub>2</sub>) radicals by aerosols, and accounting for atmospheric oxidation of volatile chemical products (VCPs). We find that the tropospheric NO<sub>2</sub> columns measured from space in the SMA are mainly contributed by the planetary boundary layer (PBL) below 2 km altitude, reflecting the highly polluted conditions. Repeated measurements of NO<sub>2</sub> vertical profiles over the SMA at different times of day show that diurnal change in mixing depth affecting the NO<sub>2</sub> vertical profile induces a diurnal variation in AMF of comparable magnitude to the diurnal variation in the NO<sub>2</sub> column. GEOS-Chem captures this diurnal variation in AMF and more generally the variability in the AMF for the KORUS-AQ NO<sub>2</sub> vertical profiles (2.7% mean bias, 7.6% precision), with some outliers in the morning due to errors in the timing of mixed layer growth.

Deleted: Tropospheric nitrogen dioxide (

Deleted: is

Deleted: high-density

Deleted: data including

Formatted: Subscript

Deleted: over East Asia

Deleted: AMF and its variability.

Deleted: non-systematic

## 1. Introduction

Nitrogen [oxides](#) ( $\text{NO}_x \equiv \text{NO} + \text{NO}_2$ ) are emitted by fuel combustion and from natural sources such as lightning, wildfires, and soils. They play a critical role in driving atmospheric oxidant chemistry with implications for air quality and health, climate forcing, and nitrogen deposition to ecosystems. Satellite-based retrievals of tropospheric  $\text{NO}_2$  columns have been used extensively to investigate  $\text{NO}_x$  emissions and their trends (Richter et al., 2005; Stavrou et al., 2008) and  $\text{NO}_x$  atmospheric lifetime (de Foy et al., 2015; Laughner and Cohen, 2019). The retrievals require local  $\text{NO}_2$  vertical profile information to account for atmospheric scattering, but there can be large uncertainties in these profiles (Travis et al., 2016). The Geostationary Environment Monitoring Spectrometer (GEMS) launched in February 2020 is now [providing](#) continuous [hourly](#)  $\text{NO}_2$  column observations over East Asia (J. Kim et al., 2020; J. Park et al., 2022). Here we use observations from the Korea-United States Air Quality (KORUS-AQ) aircraft campaign together with GEOS-Chem chemical transport model (CTM) simulations to better understand the factors controlling  $\text{NO}_2$  vertical profiles over East Asia, their relations to the broader photochemical environment, and the implications for [observing the diurnal variation of  \$\text{NO}\_2\$  from GEMS](#).

Tropospheric  $\text{NO}_2$  has been measured from polar sun-synchronous low-earth orbiting (LEO) satellite instruments since 1995 with the Global Ozone Monitoring Experiment (GOME) (1995-2003; Burrows and Chance, 1993; Martin et al., 2002) continued by the Scanning Imaging Spectrometer for Atmospheric Chartography (SCIAMACHY) (2002-2012; Bovensmann et al., 1999), GOME-2 (2006-; Callies et al., 2000), the Ozone Monitoring Instrument (OMI) (2004-; Levelt et al., 2018), the Ozone Mapping Profiler Suite (OMPS) (2011-; Flynn et al., 2014), the Tropospheric Monitoring Instrument (TROPOMI) (2017-; Veefkind et al., 2012), and the Environmental Trace Gases Monitoring Instrument (EMI) (2018-; Zhang et al., 2018). GEMS is the first geostationary instrument [to measure tropospheric  \$\text{NO}\_2\$](#) . The retrievals fit the backscattered solar spectra in the 400-470 nm wavelength range to obtain a  $\text{NO}_2$  slant column density (SCD) from which the stratospheric portion is removed [to estimate the tropospheric SCD](#) (Bucsela et al., 2013; Boersma et al., 2018). The tropospheric SCD is then converted to a vertical column density (VCD) with an air mass factor (AMF) for the scattering atmosphere that depends on the shape of the local  $\text{NO}_2$  vertical profile (Palmer et al., 2001; Eskes and Boersma, 2003). The vertical profile varies locally as a function of emissions, chemistry, and meteorology and must therefore be provided [independently](#) by a CTM. Model errors in that vertical profile can be a major contributor to the VCD error budget (Martin et al., 2002; J. Lin et al., 2012; Boersma et al., 2018).

Deleted: oxide radicals

Deleted: starting to provide

Deleted: including diurnal variation

Deleted: GEMS retrievals.

Formatted: Font: Times

The LEO instruments [observe](#) NO<sub>2</sub> once a day at a particular local time of day, but tropospheric NO<sub>2</sub> VCDs vary with the time of day as driven by emissions [and](#) chemistry. Previous studies obtained some sparse information on this diurnal variation by using the difference in overpass time between two LEO satellites. 85 Boersma et al. (2008) used SCIAMACHY and OMI and found higher tropospheric NO<sub>2</sub> VCDs in mid-morning than in the early afternoon over polluted regions, [which they attributed to](#) photochemical loss over the course of the day. J. Lin et al. (2010) used the [combination](#) of GOME-2 and OMI for a top-down estimate of NO<sub>x</sub> emissions over China including diurnal variation. Penn and Holloway (2020) found that NO<sub>2</sub> column ratios between morning and afternoon are lower than surface NO<sub>2</sub> concentration ratios, as would be expected 90 from deeper vertical mixing in the afternoon, but with [large](#) heterogeneity in the ratio at the urban scale. The hourly data from GEMS should enable a better understanding of [the diurnal patterns of NO<sub>2</sub>](#) and an opportunity to better account for the diurnal variation of NO<sub>x</sub> emissions and chemical lifetime.

The role of oxidant chemistry in controlling NO<sub>2</sub> [concentration](#) and its vertical profile is of particular interest. This chemistry involves ozone (O<sub>3</sub>), hydrogen oxide radicals (HO<sub>x</sub> ≡ OH + peroxy radicals), and volatile 95 organic compounds (VOCs), which control the NO/NO<sub>2</sub> partitioning and the atmospheric lifetime of NO<sub>x</sub>. CTM errors in describing oxidant chemistry can result in large errors in NO<sub>2</sub> profiles (Travis et al., 2016; Silvern et al. 2018). R. Park et al. (2021) found that the O<sub>3</sub> concentrations observed in KORUS-AQ were severely underestimated by CTMs and this would affect the simulation of the NO/NO<sub>2</sub> ratio.

The KORUS-AQ campaign deployed the NASA DC-8 aircraft over and around the Korean peninsula in May- 100 June 2016 with vertical profiling at up to 7 km altitude (Crawford et al., 2021). The aircraft carried a large payload of instrumentation for oxidant chemistry. Previous relevant analyses of the KORUS-AQ data focused on comparisons to an ensemble of CTMs (R. Park et al., 2021), investigations of the factors controlling CO and O<sub>3</sub> (Gaubert et al., 2020; Schroeder et al., 2020), heterogeneous chemistry (Heim et al., 2020; Brune et al., 2022), VOCs reactivity (Simpson et al., 2020), aerosol nitrate photolysis (Romer et al., 2018), and aerosol 105 composition (Nault et al., 2018; H. Kim et al., 2018; Jordan et al., 2020), along with a number of GEOS-Chem-specific studies referenced in Section 2.

Here we conduct simulations of the KORUS-AQ observations using GEOS-Chem at 0.25 ° × 0.3125° resolution with recent chemical updates including aerosol nitrate (NO<sub>3</sub><sup>-</sup>) photolysis (Shah et al., [2023](#)), coarse particulate matter uptake of nitric acid (HNO<sub>3</sub>) (Zhai et al., [2023](#)), emissions of volatile 110 chemical products (VCPs) (Bates et al., 2022) and revision of HO<sub>2</sub> heterogeneous uptake by aerosols. As we will see, these updates enable a much-improved representation of oxidant chemistry relative to previous GEOS-Chem versions, [which provides a basis for model](#) evaluation with observed NO<sub>2</sub> concentrations and NO/NO<sub>2</sub> ratios. We go on to examine the diurnal variation of [NO<sub>2</sub> vertical profiles and the resulting diurnal](#)

Deleted: observed

Deleted: ,

Deleted: , and mixing depth

Deleted: mainly driven by

Deleted: diurnal variation

Deleted: NO<sub>2</sub> as observed by

Deleted: significant

Deleted: These diurnal variations inferred from LEO satellite data seem however inconsistent with observations from ground-based Pandora spectrometers over South Korea, which show flat tropospheric NO<sub>2</sub> VCDs between mid-morning and afternoon (Chong et al., 2018; Crawford et al., 2021). ...

Deleted: this issue

Deleted: 2022

Deleted: 2022a

Deleted: . We start from an

Deleted: of the model

Deleted: vertical profiles of O<sub>3</sub> and HO<sub>x</sub> species which leads us to evaluation with observations of

Deleted: , NO,

Deleted: the

variation of AMF as defined by [the observations](#) and [by GEOS-Chem](#), and from there quantify the [AMF errors associated with retrieving NO<sub>2</sub> diurnal variations from GEMS using GEOS-Chem vertical profiles](#).

- Deleted: observed
- Deleted: vertical profiles
- Deleted: to compute the AMFs for GEMS retrievals

## 2. Methods

### 2.1. KORUS-AQ observations

140 KORUS-AQ included 20 research flights with the NASA DC-8 aircraft, all based out of Osan Air Base and covering South Korea and the adjacent ocean with a particular focus on the Seoul Metropolitan Area (SMA) (Crawford et al., 2021). All flights were in the 08 – 16 local time (LT) window. We exclude observations made near Daesan (36.4 – 37.15°N, 126 – 126.88°E) that focused on sampling power plant plumes. We use a 60-second merged dataset of the aircraft observations (available at <https://www-air.larc.nasa.gov/>). We  
145 sample the GEOS-Chem model along the flight tracks at the time of the observations. Comparisons of the model to observations are presented after averaging the observations along the flight tracks over the model grid.

Specific KORUS-AQ aircraft measurements used in this work include [Thermal Dissociation Laser-Induced Fluorescence](#) (TD-LIF) for NO<sub>2</sub> concentrations (Thornton 2000; Nault et al., 2015), NCAR 4-Channel  
150 NO<sub>x</sub>O<sub>3</sub>Chemiluminescence for NO and O<sub>3</sub> concentrations (Walega et al. 1991), NCAR CCD-based Actinic Flux Spectrometer (CAFS) for NO<sub>2</sub> photolysis frequencies ( $j_{\text{NO}_2}$ ), airborne tropospheric hydrogen oxides sensor (ATHOS) for OH and HO<sub>2</sub> concentrations and OH reactivity (OHR) (Faloona et al., 2004; Mao et al., 2009), Differential Absorption Carbon monOxide Measurement (DACOM) for CO concentrations (Sachse et al., 1987), [High-Resolution Time-of-Flight Aerosol Mass Spectrometer](#) (CU HR-ToF-AMS) for sulfate,  
155 nitrate, and ammonium aerosols (DeCarlo et al., 2006; Nault et al., 2018) and [CF<sub>3</sub>O<sup>-</sup> Chemical Ionization Time of Flight Mass Spectrometer](#) (CIT-ToF-CIMS) for H<sub>2</sub>O<sub>2</sub> concentrations (Crounse et al., 2006). [The stated uncertainties for these measurements are 5% for NO<sub>2</sub>, 30 pptv + 20% for NO, 5 ppbv + 10% for O<sub>3</sub>, 12% for  \$j\_{\text{NO}\_2}\$ , 32% for HO<sub>x</sub>, 0.8 s<sup>-1</sup> for OHR, 2% \(or 2 ppbv\) for CO, 34% for sulfate, nitrate, and ammonium aerosols, and 30% for H<sub>2</sub>O<sub>2</sub>](#). Both TD-LIF and NO<sub>x</sub>O<sub>3</sub>Chemiluminescence measured NO<sub>2</sub> concentrations,  
160 and both are known for positive interferences at high altitudes from CH<sub>3</sub>O<sub>2</sub>NO<sub>2</sub> and HNO<sub>4</sub> dissociation (Reed et al., 2016; Nussbaumer et al., 2021). [We use the TD-LIF measurements in this work since they detect NO<sub>2</sub> directly and attempt](#) to correct for positive interference (Nault et al., 2015). We also use surface NO<sub>2</sub> concentrations from a Teledyne T500U CAPS analyzer located at Olympic Park in the SMA.

- Deleted: thermal dissociation laser-induced fluorescence

- Deleted: A high

- Deleted: a

- Deleted: Since

- Deleted: data attempts

- Deleted: and detect NO<sub>2</sub> directly

- Deleted: ), TD-LIF NO<sub>2</sub> is used for this work.

- Formatted: Font: Not Bold

### 2.2. GEOS-Chem model

175 We use GEOS-Chem version 13.3.4 ([v13.3.4; https://doi.org/10.5281/zenodo.5764874](https://doi.org/10.5281/zenodo.5764874), last accessed 20  
March 2022) driven by the Goddard Earth Observing System - Forward Processing (GEOS-FP) assimilated  
meteorological data with a horizontal resolution of  $0.25^\circ \times 0.3125^\circ$  and 72 vertical levels up to the  
mesopause including 14 levels below 2 km altitude. The native resolution is used over the Korean peninsula  
and surrounding ocean ( $29^\circ - 40^\circ\text{N}$ ,  $120^\circ - 135^\circ\text{E}$ ) with dynamic boundary conditions updated every three  
180 hours from a global  $4^\circ \times 5^\circ$  simulation. The simulation is conducted for April-June 2016 following 6 months  
of initialization. Emissions in GEOS-Chem are calculated by the Harmonized Emissions Component  
(HEMCO) (H. Lin et al., 2021). Global anthropogenic emissions are from the Community Emissions Data  
System (CEDSV2) (McDuffie et al., 2021), superseded in China by the Multi-resolution Emission Inventory  
(MEIC; Zheng et al., 2018), and for the rest of Asia including shipping by the KORUSv5 inventory (Woo et  
185 al., 2020). We apply a diurnal profile of  $\text{NO}_x$  emission rates derived from an emission inventory for the SMA  
(Goldberg et al., 2019). Natural emissions are from Guenther et al. (2012) for biogenic VOCs (MEGANv2),  
Murray et al. (2012) for lightning  $\text{NO}_x$ , Hudman et al. (2012) for soil  $\text{NO}_x$ , and Jaeglé et al. (2011) for sea-  
salt aerosol (SSA) as  $\text{Na}^+$ . GEOS-Chem v13.3.4 includes a detailed oxidant-aerosol chemical mechanism  
with recent updates for halogen chemistry (Wang et al., 2021),  $\text{NO}_x$  heterogeneous and cloud chemistry  
(Holmes et al., 2019), isoprene chemistry (Bates and Jacob, 2019), and aromatic chemistry (Bates et al.,  
190 2021). We introduce additional updates as described below.

Several previous studies have used GEOS-Chem to simulate and interpret KORUS-AQ observations. Choi  
et al. (2019) studied local and transboundary sources of fine particulate matter ( $\text{PM}_{2.5}$ ). Zhai et al. (2021)  
analyzed aerosol vertical profiles for the interpretation of satellite aerosol optical depth (AOD) observations.  
195 Travis et al. (2022) found a large model overestimate of nitrate and underestimate of sulfate aerosols. R. Park  
et al. (2021) showed systematic low biases in simulated CO and  $\text{O}_3$  concentrations at all altitudes. Oak et al.  
(2019) found that correcting the daytime planetary boundary layer (PBL) height and increasing  $\text{NO}_x$  emission  
(since corrected in the KORUSv5 inventory) led to a more accurate simulation of surface  $\text{O}_3$  concentration.  
H. Kim et al. (2022) found that simulated OHR was too low and attributed this to underestimates of CO and  
200 oxygenated VOC (OVOC) emissions. Model comparison to formaldehyde (HCHO) observations from the  
aircraft also found an underestimate in emissions of anthropogenic VOCs (aVOCs) (Kwon et al., 2021).

Here we make four updates to the standard GEOS-Chem model to better represent the oxidant chemistry over  
South Korea: (1) addition of  $\text{NO}_3^-$  photolysis, (2) uptake of  $\text{HNO}_3$  by coarse anthropogenic dust, (3) VCP  
emissions, and (4)  $\text{HO}_2$  heterogeneous uptake by aerosols. We describe each of them in order.

205 We incorporate  $\text{NO}_3^-$  photolysis in the model following Shah et al. (2023). Observations in marine air show  
high nitrous acid (HONO) concentrations that have been attributed to  $\text{NO}_3^-$  photolysis with support from

Deleted: (

Deleted: in GEOS-Chem

Deleted: version 13.3.4 (

Deleted: )

Deleted: (Wang et al., 2019; R. Park et al., 2004)

Deleted: 2022

laboratory experiments in particular for Cl-containing aerosol (Zhou et al., 2008; Ye et al., 2016; Reed et al., 2017). Kasibhatla et al. (2018) initially added  $\text{NO}_3^-$  photolysis in coarse sea salt aerosol (SSA) as an option in GEOS-Chem. Shah et al. (2023) extended this to all  $\text{NO}_3^-$  aerosols to correct a low model bias for  $\text{NO}_x$  concentrations in the remote troposphere. They express the  $\text{NO}_3^-$  photolysis frequency ( $j_{\text{NO}_3^-}$ ) as the  $\text{HNO}_3$  photolysis frequency ( $j_{\text{HNO}_3}$ ) multiplied by an enhancement factor (EF):  $j_{\text{NO}_3^-} = \text{EF} \times j_{\text{HNO}_3}$ . An EF of 100 is applied for coarse-mode ( $>1 \mu\text{m}$ ) sea-salt  $\text{NO}_3^-$  aerosol. For fine mode  $\text{NO}_3^-$  aerosol, which in GEOS-Chem is an internal mixture of sulfate-nitrate-ammonium (SNA) and fine sea-salt, the EF is calculated using equation (1):

$$\text{EF} = \max\left(100 \times \frac{1}{1 + \frac{[\text{NO}_3^-]}{[\text{SSA}]}} , 10\right) \quad (1)$$

where [ ] denotes a molar concentration and  $[\text{SSA}] = 2.39[\text{Na}^+]$  ( $\text{Na}^+$  is the inert SSA tracer in GEOS-Chem). Our resulting mean EF value for the fine mode  $\text{NO}_3^-$  aerosol along the KORUS-AQ flight tracks is 15. Romer et al. (2018) inferred a non-SSA EF value in the range of 1-30 from the ratio of  $\text{NO}_x$  to total inorganic nitrate concentrations measured in KORUS-AQ over the Yellow Sea.

We add  $\text{HNO}_3$  uptake by anthropogenic coarse particulate matter ( $\text{PM}_{10} - \text{PM}_{2.5}$ ) following Zhai et al. (2023). Coarse particulate matter measured by the surface air quality network in South Korea is on average  $20 \mu\text{g m}^{-3}$ , and most is anthropogenic fugitive dust that would take up  $\text{HNO}_3$  similarly to natural dust (Fairlie et al., 2010). Zhai et al. (2023) found that they could correct in this manner most of the previously identified high model biases for  $\text{HNO}_3$  and  $\text{NO}_3^-$  during KORUS-AQ.

Non-industrial VCPs (e.g., adhesives, cleaning agents, coatings, pesticides, printing inks, and personal care products) are missing from the KORUSv5 emission inventory. We add them here based on per capita emission estimates from McDonald et al. (2018) and Coggon et al. (2021), as incorporated into GEOS-Chem by Bates et al. (2022). Observations in the SMA suggest that these VCP emissions are important (S. Kim et al., 2016; Simpson et al., 2020), and we find in GEOS-Chem that they account for 97% of ethanol anthropogenic emissions, 94% of acetone, 31% of toluene, and 90% of methanol. The VCPs are emitted following a diurnal emission profile from Coggon et al. (2021). Oxidation of VCP ethanol is a major source of acetaldehyde for the conversion of  $\text{NO}_x$  to peroxyacetyl nitrate (PAN) (Zhai et al., 2022). Oak et al. (2019) and Schroeder et al. (2020) found toluene to dominate  $\text{O}_3$  production in the SMA.

Finally, we decrease the reactive uptake coefficient  $\gamma$  of  $\text{HO}_2$  ( $\gamma_{\text{HO}_2}$ ) by aerosols to 0.1, as compared to 0.2 in the standard GEOS-Chem model (Martin et al., 2003; Mao et al., 2010). As we will show in Section 3,  $\gamma_{\text{HO}_2} = 0.1$  gives a better fit to the  $\text{HO}_2$  observations and their relationship to aerosol concentrations in KORUS-AQ.

Deleted: 2022

Deleted: The

Deleted: is computed as an enhancement factor (EF) relative to...

Deleted: ):

Deleted: ×

Formatted: Font: Cambria Math

Deleted: 2022a

Deleted: very high, averaging

Deleted: are

Deleted: 2022a

Deleted: in the daytime though there remains nighttime overestimate (Zhai et al., 2021; Travis et al., 2022).

Deleted: We implement VOC emissions from non

Deleted: uses of volatile chemical products (

Deleted: )

Deleted: The KORUSv5 inventory does not account for non-industrial VCP emissions but observations

Deleted: they

Deleted: 2022b

Deleted: Toluene emission increases by 44% when including VCPs. ...

Brune et al. (2022) used a box model to show that  $\gamma_{\text{HO}_2} = 0.2$  is too high for simulating HO<sub>2</sub> observations in  
 265 KORUS-AQ. A  $\gamma_{\text{HO}_2}$  value of 0.1 is within the range of current knowledge (Lakey et al., 2015; Zou et al.,  
 2019; Taketani et al., 2012). Reactive uptake of HO<sub>2</sub> by aerosol can have either H<sub>2</sub>O or H<sub>2</sub>O<sub>2</sub> as a product,  
 and GEOS-Chem assumes H<sub>2</sub>O by default to avoid overestimation of H<sub>2</sub>O<sub>2</sub> observations (Mao et al., 2010;  
 2013). This is supported for the KORUS-AQ conditions by previous model studies finding that the  
 assumption of H<sub>2</sub>O<sub>2</sub> as a product of HO<sub>2</sub> heterogeneous uptake leads to a large overestimate of observed  
 270 H<sub>2</sub>O<sub>2</sub> concentrations (Miyazaki et al., 2019; Gaubert et al., 2020).

Deleted: ,

Underestimation of CO in the northern hemisphere is a common problem for CTMs (Shindell et al., 2006;  
 Huijnen et al., 2010) and this was also found for GEOS-Chem in KORUS-AQ throughout the tropospheric  
column (R. Park et al., 2021; H. Kim et al., 2022). This could be due to missing CO sources in East Asia  
(Gaubert et al., 2020; R. Park et al., 2021) missing VOC emissions (Huijnen et al., 2010), and/or excessive  
 275 OH concentrations (Naik et al., 2013). Here we find that a 50% increase at all altitudes in the GEOS-Chem  
CO concentrations used as boundary conditions corrects the model bias for simulating KORUS-AQ  
observations. We adopt this correction in our simulation.

Deleted: (R.

Deleted: simply implement

Deleted: to overcome

Deleted: underestimation

### 2.3. Air Mass Factor (AMF) Calculation

The AMF is a crucial component of satellite retrievals of the tropospheric NO<sub>2</sub> VCD  $\Omega_v$  (molecules cm<sup>-2</sup>).  
 280 Spectral fitting of backscattered radiances along the line of sight of the instrument measures a total  
atmospheric SCD, from which the stratospheric contribution is removed to yield a tropospheric NO<sub>2</sub> SCD  $\Omega_s$ .  
The AMF then applies a radiative transfer model together with independent information on the NO<sub>2</sub> vertical  
profile to derive  $\Omega_v$ :

Deleted: Satellite retrieval

Deleted: ) applies an AMF for the scattering atmosphere to the tropospheric NO<sub>2</sub> SCD  $\Omega_s$  measured

Deleted: by the spectral fitting of the backscattered radiances and subtracting

Deleted: :

$$\Omega_v = \Omega_s / \text{AMF} \quad (2)$$

285 The AMF depends on the viewing geometry, the scattering properties of the surface and the atmosphere, and  
 the vertical distribution of NO<sub>2</sub>, as given by Palmer et al. (2001):

$$\text{AMF} = \text{AMF}_G \int_0^{z_T} w(z) S(z) dz \quad (3)$$

Here AMF<sub>G</sub> is the geometric AMF assuming no atmospheric scattering and is a function of solar zenith angle  
 (SZA) and viewing zenith angle (VZA);  $w(z)$  is a scattering weight that measures the relative sensitivity of  
 290 the backscattered radiance measured from space to the NO<sub>2</sub> optical depth at altitude  $z$ , averaged over the  
 wavelength range of the spectral fitting window (Lamsal et al., 2021);  $S(z) = n(z)/\Omega_v$  is a shape factor for the  
 vertical distribution of the NO<sub>2</sub> number density  $n(z)$ ; and the integration is from the surface to the tropopause  
 $z_T$ . The scattering weights are such that  $w(z) = 1$  for all  $z$  in a non-scattering atmosphere, in which case AMF

Formatted: Font: Not Italic



305 =  $AMF_G$  is solely defined by the geometric light path from the Sun to the satellite as reflected by the surface. We will refer to  $\int_0^{\tau} w(z)S(z)dz$  in what follows as the scattering correction factor.

Here we use shape factors  $S(z)$  from the KORUS-AQ vertical profiles, either observed from the aircraft or simulated with GEOS-Chem, to compute the AMF. The scattering weights  $w(z)$  are obtained from the OMI NO<sub>2</sub> retrieval lookup table (LUT) as a function of SZA, VZA, relative azimuth angle (RAA), surface pressure, and albedo (Bucsela et al., 2006; 2013). We compute SZA, VZA, and RAA for the locations and times of the KORUS-AQ aircraft profiles and the geostationary location of the GEMS satellite instrument (128°E longitude, 0° latitude, 35786 km mean altitude). We assume a surface pressure of 1013 hPa. The surface albedo is determined from OMI Level-3 LER climatology (OMLER; Kleipool et al., 2008) for June and the locations of the KORUS-AQ profiles. The tropopause is assumed to be at 12 km altitude, but results are insensitive to that assumption because the bulk of the NO<sub>2</sub> tropospheric column is in the PBL.

Our specific interest in computing AMFs for the KORUS-AQ conditions is for application to GEMS retrievals. The spectral retrieval windows for OMI (402 – 465 nm) and GEMS (432 – 450 nm) have a sufficient overlap that we can assume the scattering weights to be similar for our analysis, considering that the wavelength dependence of scattering weights is weak (Palmer et al., 2001). We focus our attention on clear-sky scenes for a Rayleigh atmosphere without aerosol scattering. Retrieval for partly cloudy scenes in the GEMS algorithm uses a cloud albedo (0.8) instead of the surface albedo for the cloudy fraction of the scene, assumes  $w(z) = 0$  below cloud top, and weighs the clear-sky and cloudy scattering weights by their relative contributions to the back-scattered radiances (Martin et al., 2002; Lee et al., 2020). Our focus on clear-sky scenes does not detract from the generality of our results, since the extension to partly cloudy scenes is straightforward, except for the possible role of the cloud in altering the NO<sub>2</sub> vertical profile but this is generally not considered in retrieval algorithms.

### 3. Results and Discussion

#### 3.1. Oxidant chemistry and NO<sub>x</sub> vertical profiles during KORUS-AQ

Figure 1 shows the relationship between HO<sub>2</sub> and sulfate-nitrate-ammonium (SNA) aerosol concentrations as observed in KORUS-AQ (panel A) and simulated by GEOS-Chem (panels B and C). The model with  $\gamma_{HO_2} = 0.2$  (panel B) shows depression of HO<sub>2</sub> concentrations at high aerosol concentrations when uptake by aerosol is the dominant HO<sub>x</sub> sink but that depression is not seen in the observations. The model with  $\gamma_{HO_2} = 0.1$  (panel C) corrects this behavior. Figure 2 shows the median simulated (red line) and observed (black line) vertical profiles of oxidants and related quantities in the SMA during KORUS-AQ, highlighting the effects

Deleted: Bucsela et al.,

Deleted: will limit

Deleted: to

Deleted: the

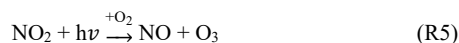
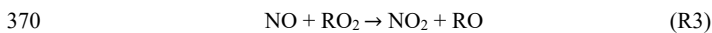
Deleted: .



340 of model updates over the standard GEOS-Chem v13.3.4 (blue line). Results outside the SMA are in Figure S1 and show similar behavior.

We see from Figure 2 that the low O<sub>3</sub> background bias previously reported by R. Park et al. (2021) is largely corrected, mainly from the inclusion of NO<sub>3</sub><sup>-</sup> photolysis in the global simulation [used as boundary conditions](#) (Shah et al., [2023](#)). The simulated O<sub>3</sub> enhancement in the PBL below 2 km matches observations much better than GEOS-Chem v13.3.4 and this is mostly driven by higher HO<sub>2</sub> concentrations, with some additional contribution from VCPs and higher CO [reflected in](#) the OHR. The higher HO<sub>2</sub> concentrations relative to GEOS-Chem v13.3.4 are due to a combination of slower heterogeneous uptake, the addition of VCP emissions, feedback from increasing O<sub>3</sub>, and an increase in CO concentrations. Sensitivity simulations show 350 that each of these factors contributes a 1 – 2 pptv increase in HO<sub>2</sub> concentration. An increase in HO<sub>2</sub> concentration drives an increase in H<sub>2</sub>O<sub>2</sub> concentration, which was previously underestimated by 21% in the PBL ([averaging over altitudes below 2 km](#)) and is now overestimated by 42%. An increase in the H<sub>2</sub>O<sub>2</sub> deposition velocity could reconcile the model and observations (Allen et al., 2022). Simulated OH concentrations are 31% higher than observed ([averaging over all altitudes](#)), which is still within the accuracy 355 of the measurement; there is little difference between our simulation and GEOS-Chem v13.3.4 for OH because higher HO<sub>x</sub> concentrations are offset by an increase in the OHR. The OHR is still lower than observed (H. Kim et al., 2022).

Figure 3 shows the median simulated (red line for GEOS-Chem; blue line for GEOS-Chem v13.3.4) and observed (black line) vertical profiles of NO ([panel A](#)) and NO<sub>2</sub> ([panel B](#)) concentrations in the SMA, 360 together with the NO/NO<sub>2</sub> concentration ratios ([panel C](#)). The same plot outside the SMA is shown in Figure S2 and the conclusions regarding the NO/NO<sub>2</sub> ratio are similar. NO and NO<sub>2</sub> are mainly in the PBL. The model underestimates NO<sub>2</sub> concentrations slightly in the SMA, which could have to do with the 25-km spatial resolution since that underestimate is not seen outside the SMA. [There is no significant difference in simulated NO<sub>2</sub> concentrations between our updated GEOS-Chem model and the standard GEOS-Chem version 13.3.4, but our updated model provides a better simulation of the observed NO/NO<sub>2</sub> ratio.](#) 365 The NO/NO<sub>2</sub> ratio is expected to be governed in the daytime by a photostationary steady state (PSS) between the fast oxidation of NO and photolysis of NO<sub>2</sub>:



Deleted: 2022

Deleted: boosting

Deleted: ,

Deleted: .

where RO<sub>2</sub> denotes organic peroxy radicals and X denotes halogens. PSS is then defined by

$$PSS = \frac{[NO]}{[NO_2]} = \frac{j_{NO_2}}{k_{NO+O_3}[O_3] + k_{NO+HO_2}[HO_2] + \sum k_{NO+RO_2}[RO_2] + \sum k_{NO+XO}[XO]} \quad (4)$$

where [ ] denotes number density, *k* denotes rate constants (Burkholder et al., 2020), and the summations  $\Sigma$  are applied to all RO<sub>2</sub> or XO species. Figure 3 panel C shows the PSS (gold line) computed from aircraft measurements except for [XO] and [RO<sub>2</sub>] which are from GEOS-Chem but contribute generally less than 4% of the conversion from NO to NO<sub>2</sub>.

We see from Figure 3 panel C that the NO/NO<sub>2</sub> ratio increases with altitude, which largely reflects the temperature dependence of the NO + O<sub>3</sub> reaction (Burkholder et al., 2020). Our updated model closely tracks the PSS, but the observations deviate above 5 km. This may be attributed to positive artifacts in the TD-LIF NO<sub>2</sub> instrument at low temperatures (Shah et al., 2023). We conclude that the PSS assumption applied to the more accurate NO concentration measurements provides a better estimate of NO<sub>2</sub> concentrations above that altitude. Hereafter, we replace the NO<sub>2</sub> observations above 5 km altitude with values inferred from the observed NO concentrations and PSS.

### 3.2. Air mass factors for satellite NO<sub>2</sub> retrievals and their diurnal variation

Figure 4 shows the median vertical profile of simulated (red line), observed (black line), and standard GEOS-Chem v13.3.4 (blue line) NO<sub>2</sub> number density in the SMA during KORUS-AQ (panel B), along with the scattering weights for satellite retrievals (panel A) and the cumulative vertical contributions to the tropospheric slant column as would be detected from a satellite instrument (panel C). No observations are available above 7 km and GEOS-Chem is used there instead. The differences between our updated GEOS-Chem simulation and the standard GEOS-Chem v13.3.4 are minuscule. The clear-sky scattering weights (panel A) represent the sensitivity of the instrument to NO<sub>2</sub> as a function of altitude and increase by a factor of 2.4 from the surface to 6 km altitude because of Rayleigh scattering. The fractional cumulative contribution to the tropospheric slant column density ( $\Omega_s$  in equation (2)) is calculated as  $\int_0^z w(z)n(z)dz / \int_0^T w(z)n(z)dz$  and represents the fraction of the measured column contributed by NO<sub>2</sub> below altitude *z*. NO<sub>2</sub> in the PBL below 2 km contributes 95% of the SCD over the SMA and 80% of the SCD for the ensemble of KORUS-AQ observations, reflecting the highly polluted conditions (panel C). Previous work over the southeastern US in the summer found that the PBL contributed only 20-35% of the SCD (Travis et al., 2016), complicating the inference of NO<sub>x</sub> emissions from NO<sub>2</sub> satellite observations (Silvern et al., 2019; Qu et al., 2021). This is much less of an issue for South Korea. The AMF inferred from the median observed NO<sub>2</sub> vertical profile in the SMA during KORUS-AQ is 1.18, in close agreement with the corresponding value of 1.22 from GEOS-Chem.

Deleted: summation

Deleted: is

Deleted: The

Deleted: 2022). This implies

Deleted: concentrations

Deleted: ) and

Deleted: ,

Deleted: .

Deleted: Observed NO<sub>2</sub>

Deleted: 5

Deleted: 7 km is inferred from NO observations using PSS.

Deleted: left

Deleted: .

Deleted: .

Deleted: such that

Deleted: large contribution from the free tropospheric background had to be considered when inferring

Deleted: the

Deleted: columns

GEMS offers the first opportunity to directly observe the diurnal variation of  $\text{NO}_2$  from space, but it is important to understand how much the AMF contributes to this diurnal variation and how well this is resolved by the model used to obtain shape factors. During the KORUS-AQ campaign, repeated flights in the morning (8 – 9 LT), midday (12 – 13 LT), and afternoon (15 – 16 LT) were conducted on 10 days over two supersites: Olympic Park (37.5232°N, 127.1260°E) and Mt. Taewha (37.3123°N, 127.3106°E) (Crawford et al., 2021). Olympic Park is in the SMA, and Mt. Taewha is a research forest site 29 km southeast of Olympic Park. Mt. Taewha is affected by SMA air pollution through downwind transport. The flight patterns involved missed landing approaches to very low flight altitudes over Olympic Park followed by spiral ascents to the east of Mt. Taewha up to 7 km altitude (Crawford et al., 2021). To construct the diurnal variation of the  $\text{NO}_2$  vertical profile over the SMA and its implication for the AMF, we combine the Olympic Park vertical profiles (typically  $z < 2\text{km}$ ) with the spirals east of Mt. Taewha. A similar approach was taken to investigate HCHO AMF using KORUS-AQ campaign data (Spinei et al., 2018). We also use the surface  $\text{NO}_2$  data from Olympic Park.

Figure 5 panel A shows the clear-sky scattering weights  $w(z)$  at 8 – 9 LT (orange line), 12 – 13 LT (purple line), and 15 – 16 LT (light blue line). In addition to the dependence on altitude, the scattering weights show a dependence on the time of day driven by the solar zenith angle (SZA) and relative azimuth angle (RAA), such that the sensitivity to near-surface  $\text{NO}_2$  at 8 – 9 LT is 14% lower than at 12 – 13 LT. Figure 5 also shows the vertical shape factors  $S(z)$  computed from the median vertical distributions of simulated (red line) and observed (black line)  $\text{NO}_2$  number densities at 8 – 9 LT (panel B), 12 – 13 LT (panel C), and 15 – 16 LT (panel D). The  $\text{NO}_2$  vertical profiles follow the rise in the mixed layer from early morning to early afternoon in response to surface heating, with higher near-surface concentrations in the morning when the mixed layer is shallow and lower surface concentrations in the afternoon due to deeper vertical mixing. Observations during KORUS-AQ indicated a mean mixed layer height at 8 – 9 LT of about 0.6 km rising to about 1.7 km in the early afternoon (Travis et al., 2022).

Although surface  $\text{NO}_2$  peaks strongly in the morning (Figure 5 panel B), the  $\text{NO}_2$  VCDs observed from ground-based sun-staring column measurements in the SMA from Chong et al. (2018) and Crawford et al. (2021) show an increase from early morning to 11 LT, steady concentrations until 14 LT, and a slight decrease afterward. Vertical mixing would not directly affect the column and the increase of the column over the morning could reflect the effect of accumulating emissions. An important difference between the ground-based and satellite measurements of  $\text{NO}_2$  columns is that there is no vertical dependence of  $\text{NO}_2$  sensitivity for the former.

Deleted: daily

Deleted: flight

Deleted: clear-sky

Deleted: ,

Deleted: KT,

Deleted: .

Deleted: Model concentrations below 1 km altitude are lower than observed, which could reflect the local urban nature of the site as compared to the 25-km grid resolution of the model.

Deleted: the

Deleted: (Chong et al., 2018; Crawford et al., 2021).

470 Table 1 shows the AMF diurnal variation inferred from the NO<sub>2</sub> vertical profiles in Figure 5 for the three  
different times of the day, (panels B, C, and D). This diurnal variation is driven by three factors: 1) the  
dependence of the light path on SZA (AMF<sub>G</sub>), 2) the dependence of the scattering weights  $w(z)$  on SZA and  
RAA, and 3) the dependence of the shape factors  $S(z)$  on the diurnal cycle of mixed layer growth. The  
scattering correction factor  $\int_0^{z^T} w(z)S(z)dz$  in Table 1 captures the combined effects of  $w(z)$  and  $S(z)$ . From a  
475 purely geometric perspective (non-scattering atmosphere), as measured by AMF<sub>G</sub>, the measurement would  
be 28% more sensitive in the morning than at midday because of the longer light path. However, this effect  
is offset by the scattering correction factor which is 17% smaller in the morning than at midday, because NO<sub>2</sub>  
in the morning is closer to the surface and therefore harder to detect. As a result, the AMF is only 7% higher  
in the morning than at midday. There is no such offsetting effect from midday to afternoon since the NO<sub>2</sub>  
480 vertical profiles are similar in midday and afternoon. Thus, the AMF in the afternoon is 14% larger than at  
midday.

Deleted: .

The relative diurnal variations of the tropospheric NO<sub>2</sub> VCDs (22%; Crawford et al., 2021) and of the  
scattering correction factor (21%) are of comparable magnitude, indicating that the diurnal variation in the  
NO<sub>2</sub> vertical profile affecting the AMF is of critical importance when interpreting the diurnal variation of  
485 VCDs from the satellite. We see from Table 1 that GEOS-Chem (given in parentheses) reproduces closely  
the observed diurnal variation of the shape factor and thus of the scattering correction factor and the AMF.

Deleted: profile-driven

Deleted: relative

Deleted: important to account for

Deleted: hence

We investigate more broadly in Figure 6 the observed variability of the AMF, and the ability of GEOS-Chem  
to reproduce it, for the 63 vertical profiles collected during KORUS-AQ. These include 41 vertical profiles  
that combine flights over Olympic Park and Mt. Taewha spirals at different times of day, 17 vertical profiles  
490 that combine flights over Osan (just south of Seoul) and Mt. Taewha spirals, and 5 vertical profiles over the  
ocean. All individual profiles extend from below 0.5 km to above 6.5 km. For the Osan and ocean profiles,  
we extend the aircraft observations from the lowest altitude to the surface as there are no surface  
measurements. Oceanic data are shown in navy, and the land data are colored by the time of day (7 – 9 LT  
in orange, 11 – 13 LT in purple, and 14 – 17 LT in light blue).

Deleted: is

Deleted: is

Deleted: depending on

Deleted: the

495 The observed AMF in Figure 6 ranges from 1.05 to 1.63, representing a major factor of variability in the  
retrieved tropospheric NO<sub>2</sub> VCDs. The two main drivers of this observed AMF variability are NO<sub>2</sub> profile  
shape, determined by the presence or absence of local sources (ocean versus land), and time of day for land.  
Oceanic profiles have higher AMF (Mean: 1.55, SD: 0.068) than land (Mean: 1.23, SD: 0.097) because the  
NO<sub>2</sub> PBL enhancement is weaker or absent. All KORUS-AQ vertical profiles over land have large NO<sub>2</sub> PBL  
500 enhancements, and time of day is then the principal driver of variability as previously discussed. GEOS-  
Chem captures 53% of the variance in the observed AMF for individual profiles, and its overall error in

Deleted: surface type

Deleted: ±

Deleted: ±

Deleted: (Martin et al., 2002).

Deleted: leading to the

Deleted: being

Deleted: driving factor

computing the AMF is relatively small with a normalized mean bias (NMB) of 2.7% and a relative root-mean-square error (RRMSE) of 7.6%. The largest discrepancies are for four early-morning profiles (7 – 9  
520 LT), which are attributable to a model error in the timing of mixed layer growth (Travis et al., 2022), being either too early (AMF overestimate) or too late (AMF underestimate).

The AMF RRMSE from using GEOS-Chem model NO<sub>2</sub> shape factors (Figure 6) can be placed in the context of other contributions to the AMF error. Boersma et al. (2007) estimated that the AMF contributes a 30% error to OMI tropospheric NO<sub>2</sub> VCD retrievals, but this included contributions from uncertainties in clouds  
525 and surface albedo. Uncertainty in the shape factors as computed from the TM4 CTM accounted for 30% of the AMF error or 9% of the overall error in the tropospheric NO<sub>2</sub> VCD. Our RRMSE of 7.6% from the use of GEOS-Chem shape factors to compute the AMF under KORUS-AQ conditions is consistent with their results and extends them to observations at different times of the day. Considering that the satellite observations are typically averaged over many days for analysis, which would reduce the RRMSE, a more  
530 important consideration is the NMB which we find to be only 2.7% with GEOS-Chem. Of most concern is that the interpretation of the diurnal variability of tropospheric NO<sub>2</sub> VCDs from space could be affected by large AMF errors in the morning hours due to incorrect model timing of mixed layer growth. In GEOS-Chem at least, this error does not appear to be systematic so averaging over multiple days would dampen it.

Our analysis focused on clear-sky conditions. Clouds may dominate the AMF error budget for cloud fractions  
535 larger than 20% corresponding to more than 50% of the observed radiance originating from the cloudy fraction of the satellite pixel (Boersma et al., 2007). The GEMS algorithm (Lee et al., 2020) computes the AMF for cloudy conditions by assuming scattering weights of zero below the cloud top. The AMF for a partly cloudy scene with radiance-weighted cloud fraction  $f$  is then obtained as

$$\text{AMF} = \text{AMF}_G \left( f \int_{z_c}^{z_T} w_c(z) S(z) dz + (1 - f) \int_0^{z_T} w(z) S(z) dz \right) \quad (5)$$

540 where  $z_c$  is the cloud top altitude and the scattering weights  $w_c$  above the cloud top are computed using the cloud albedo. Although clouds would be expected to affect the NO<sub>2</sub> vertical profile through photolysis, chemistry, and vertical motions, these effects are complex, and we do not find obvious cloud-driven differences in the model or observed NO<sub>2</sub> profiles. From a diurnal variability perspective, the afternoon formation of fair-weather cumuli would decrease the sensitivity of the satellite measurement to the PBL  
545 (which would not be detected in the cloudy fraction of the scene) and therefore alias the observed diurnal variation of NO<sub>2</sub>. The exploitation of GEMS data to interpret diurnal variations of tropospheric NO<sub>2</sub> VCDs in terms of emissions or chemistry will need to focus on conditions with small cloud fractions.

#### 4. Conclusions

Deleted: errors

Deleted: , as shown in

Deleted: ,

Deleted: with dominant

Deleted: However, it would be rare to find a 7×8 km<sup>2</sup> GEMS pixel without clouds (Remer et al., 2012).

Formatted: Font: Not Italic

Formatted: Font: Not Italic

Deleted: they are

Deleted: an

Deleted: source of error when comparing

Deleted: and

560 We used extensive observations of NO<sub>2</sub> vertical profiles and related chemistry from the KORUS-AQ aircraft  
campaign over and around South Korea in May-June 2016 to better understand how the [diurnal changes in  
the vertical distribution of NO<sub>2</sub>](#)  ~~affect the diurnal variation of~~ air mass factors (AMFs)  ~~used~~ for satellite  
retrievals of tropospheric NO<sub>2</sub> vertical column density (VCD) in the polluted East Asia chemical environment.  
This was motivated by the recent launch of the GEMS geostationary instrument over East Asia, enabling the  
565 first direct measurements of the diurnal variation of NO<sub>2</sub> from space, and by interest in using the GEOS-  
Chem chemical transport model (CTM) to provide the NO<sub>2</sub> relative vertical profiles (shape factors) needed  
for the [NO<sub>2</sub> VCD](#) retrievals. We examined more broadly the role of oxidant chemistry in controlling NO<sub>2</sub>  
concentrations in GEOS-Chem through the photostationary steady state (PSS) NO/NO<sub>2</sub> ratio and the lifetime  
of NO<sub>x</sub>.

Deleted: affects

Deleted: -time

570 We introduced several updates to GEOS-Chem to improve the model representation of oxidant chemistry  
over East Asia, drawing on previous evaluations of the standard version of the model with the KORUS-AQ  
data. The inclusion of aerosol nitrate photolysis in the model corrects the previous underestimate of the O<sub>3</sub>  
background. The standard model depleted HO<sub>2</sub> under highly polluted conditions due to uptake by aerosol  
particles but this was not seen in observations. Decreasing the HO<sub>2</sub> reactive uptake coefficient corrects this  
model behavior, and model HO<sub>2</sub> is further brought into agreement with observations by the addition of  
575 volatile chemical products (VCPs) chemistry and an increase in CO. The HO<sub>2</sub> correction in turn allows the  
model to simulate the observed O<sub>3</sub> enhancement in the planetary boundary layer (PBL) below 2 km altitude.  
Increasing O<sub>3</sub> and HO<sub>2</sub> in the model improves the simulation of the PSS NO/NO<sub>2</sub> ratio.

The KORUS-AQ vertical profiles indicate that 95% of the [cumulative slant column density \(SCD\)](#) detected  
580 from space over the Seoul Metropolitan Area (SMA) originates from the PBL, despite the much higher  
sensitivity to NO<sub>2</sub> in the free troposphere, reflecting the highly polluted conditions. [The diurnal variation of  
NO<sub>2</sub> VCD observed by GEMS](#)  ~~should thus provide direct insights on~~ NO<sub>x</sub> emissions and PBL chemistry in  
[urban areas of East Asia](#), but [this](#) requires correct accounting of the diurnal variation in AMF. KORUS-AQ  
offered a unique dataset for addressing this issue with repeated diurnal vertical profiles over [the](#) SMA at  
585 different times of the day. We find that the diurnal evolution of the NO<sub>2</sub> shape factor resulting from mixed  
layer growth drives a 21% increase in the scattering correction factor from 8 – 9 LT to 12 – 13 LT, offsetting  
the geometric decrease in the resulting AMF from the shorter light path. GEOS-Chem can capture this diurnal  
variability in the shape factor driven by mixed layer growth with no significant mean error. Incorrect timing  
of mixed layer growth can lead to large errors for individual morning profiles but averaging over a number  
of days dampens the error. [Unbiased timing of mixed layer morning growth is important for the computation  
of the diurnal variation of the AMF.](#)

Deleted: tropospheric NO<sub>2</sub> VCD

Deleted: This leads to a large

Deleted: variability

Deleted: detected from space that can be interpreted

Deleted: in terms of

The AMF values inferred from the collection of KORUS-AQ vertical profiles range from 1.05 to 1.63, with most of that variability driven by ocean versus land and by the time of day over land. GEOS-Chem captures  
600 53% of this variability in the AMF with a relative root-mean-square error (RRMSE) of 7.6% and normalized mean bias (NMB) of 2.7%. These errors are relatively small compared to other sources of retrieval errors and support the use of GEOS-Chem vertical profiles in GEMS retrievals. [Further evaluation of the GEOS-Chem NO<sub>2</sub> profiles over East Asia should be conducted with aircraft campaigns for other regions and seasons, and opportunities will arise with the ASIA-AQ campaign over Korea in the winter of 2024 \(NASA, 2021\).](#)

#### 605 **Code Availability**

The model code used in this work is available at <https://doi.org/10.5281/zenodo.5764874>.

#### **Data Availability**

The KORUS-AQ data archive is available at <https://www-air.larc.nasa.gov/> and includes both the ground-based and aircraft-based measurements (KORUS-AQ Science Team, 2019).

610

#### **Author Contribution**

The original draft preparation was done by LHY, with review and editing by DJJ, KRT, JHC, JHK, and JK. DJJ contributed to project conceptualization. Modeling was done by LHY, with additional support from NKC, SZ, KHB, VS, EB, RMY, and HL. The formal analysis was conducted by LHY with additional support from  
615 DJJ, JFB, HC, KRT, and JC. The LUT used for the scattering weights is provided by LL.

#### **Competing Interests**

The contact author has declared that none of the authors has any competing interests.

#### **Acknowledgements**

This work was funded by the Samsung Advanced Institute of Technology. [LHY was supported by a National Science Foundation Graduate Research Fellowship](#). The authors would like to acknowledge KORUS-AQ  
620 data providers including Ronald Cohen for TD-LIF, Andrew Weinheimer for NO<sub>xy</sub>O<sub>3</sub>Chemiluminescence, Samuel Hall for CAFS, William Brune for ATHOS, Glenn Diskin for DACOM, [Benjamin Nault, Pedro Campuzano-Jost, and Jose Jimenez for AMS, Paul Wennberg for CIT-CIMS, and Russell Long for CAPS,](#)

#### **References**

625 Allen, H. M., Bates, K. H., Crounse, J. D., Kim, M. J., Teng, A. P., Ray, E. A., and Wennberg, P. O.: H<sub>2</sub>O<sub>2</sub> and CH<sub>3</sub>OOH (MHP) in the Remote Atmosphere: 2. Physical and Chemical Controls, *J Geophys. Res.-Atmos.*, 127, <https://doi.org/10.1029/2021JD035702>, 2022.

Deleted: it

Commented [LY1]: Add NSF!

Deleted: measurements



- 630 Bates, K. H. and Jacob, D. J.: A new model mechanism for atmospheric oxidation of isoprene: global effects on oxidants, nitrogen oxides, organic products, and secondary organic aerosol, *Atmos. Chem. Phys.*, 19, 9613–9640, <https://doi.org/10.5194/acp-19-9613-2019>, 2019.
- Bates, K. H., Jacob, D. J., Li, K., Ivatt, P., Evans, M., Yan, Y., and Lin, J.: Development and evaluation of a new compact mechanism for aromatic oxidation in atmospheric models, *Atmos. Chem. Phys.*, 21, 18351–18374, <https://doi.org/10.5194/acp-2021-605>, 2021.
- 635 Bates, K. H., Specht, I., Jacob, D., Hornbrook, R., and Apel, E.: Sources and chemistry of ethanol, International GEOS-Chem Conference 10, St. Louis, U.S.A, 6-10 June, 2022, <https://geos-chem.seas.harvard.edu/files/acmg-geos/files/igc10-d1-p07-bates.pdf>, 2022.
- Boersma, K. F., Eskes, H. J., Veeffkind, J. P., Brinksma, E. J., Levelt, P. F., Stammes, P., Gleason, J. F., and Bucsela, E. J.: Near-real time retrieval of tropospheric NO<sub>2</sub> from OMI, *Atmos. Chem. Phys.*, 16, 2103–2118, <https://doi.org/10.5194/acp-7-2103-2007>, 2007.
- 640 Boersma, K. F., Jacob, D. J., Eskes, H. J., Pinder, R. W., Wang, J., and van der A, R. J.: Intercomparison of SCIAMACHY and OMI tropospheric NO<sub>2</sub> columns: Observing the diurnal evolution of chemistry and emissions from space, *J. Geophys. Res.*, 113, D16S26, <https://doi.org/10.1029/2007JD008816>, 2008.
- 645 Boersma, K. F., Eskes, H. J., Richter, A., De Smedt, I., Lorente, A., Beirle, S., van Geffen, J. H. G. M., Zara, M., Peters, E., Van Roozendaal, M., Wagner, T., Maasakkers, J. D., van der A, R. J., Nightingale, J., De Rudder, A., Irie, H., Pinardi, G., Lambert, J.-C., and Compernolle, S. C.: Improving algorithms and uncertainty estimates for satellite NO<sub>2</sub> retrievals: results from the quality assurance for the essential climate variables (QA4ECV) project, *Atmos. Meas. Tech.*, 11, 6651–6678, <https://doi.org/10.5194/amt-11-6651-2018>, 2018.
- 650 Bovensmann, H., Burrows, J. P., Buchwitz, M., Frerick, J., Noël, S., Rozanov, V. V., Chance, K. V., and Goede, A. P. H.: SCIAMACHY: Mission Objectives and Measurement Modes, *J. Atmos. Sci.*, 56, 127–150, [https://doi.org/10.1175/1520-0469\(1999\)056<0127:SMOAMM>2.0.CO;2](https://doi.org/10.1175/1520-0469(1999)056<0127:SMOAMM>2.0.CO;2), 1999.
- 655 Brune, W. H., Miller, D. O., Thames, A. B., Brosius, A. L., Barletta, B., Blake, D. R., Blake, N. J., Chen, G., Choi, Y., Crawford, J. H., Digangi, J. P., Diskin, G., Fried, A., Hall, S. R., Hanisco, T. F., Huey, G. L., Hughes, S. C., Kim, M., Meinardi, S., Montzka, D. D., Pusede, S. E., Schroeder, J. R., Teng, A., Tanner, D. J., Ullmann, K., Walega, J., Weinheimer, A., Wisthaler, A., and Wennberg, P. O.: Observations of atmospheric oxidation and ozone production in South Korea, *Atmos. Environ.*, 269, 118854, <https://doi.org/10.1016/j.atmosenv.2021.118854>, 2022.
- 660 Bucsela, E. J., Celarier, E. A., Wenig, M. O., Gleason, J. F., Veeffkind, J. P., Boersma, K. F., and Brinksma, E. J.: Algorithm for NO<sub>2</sub> vertical column retrieval from the ozone monitoring instrument, *IEEE T. Geosci. Remote Sens.*, 44, 1245–1258, <https://doi.org/10.1109/TGRS.2005.863715>, 2006.
- Bucsela, E. J., Krotkov, N. A., Celarier, E. A., Lamsal, L. N., Swartz, W. H., Bhartia, P. K., Boersma, K. F., Veeffkind, J. P., Gleason, J. F., and Pickering, K. E.: A new stratospheric and tropospheric NO<sub>2</sub>; retrieval algorithm for nadir-viewing satellite instruments: applications to OMI, *Atmos. Meas. Tech.*, 6, 2607–2626, <https://doi.org/10.5194/amt-6-2607-2013>, 2013.
- 665 Burkholder, J. B., Sander, S. P., Abbatt, J. P. D., Barker, J. R., Cappa, C., Crounse, J. D., and Dibble, T. S.: Chemical kinetics and photochemical data for use in atmospheric studies; evaluation number 19, NASA Jet Propulsion Laboratory, <http://hdl.handle.net/2014/49199>, 2020.
- 670 Burrows, J. P. and Chance, K. V.: SCIAMACHY and GOME: The scientific objectives, *Optical Methods in Atmospheric Chemistry*, 1715, 502–512, <https://doi.org/10.1117/12.140201>, 1993.
- Callies, J., Corpaccioli, E., Eisinger, M., Hahne, A., and Lefebvre, A.: GOME-2-Metop's Second-Generation Sensor for Operational Ozone Monitoring, *ESA bulletin*, 102, 2000.

- 675 Choi, J., Park, R. J., Lee, H.-M., Lee, S., Jo, D. S., Jeong, J. I., Henze, D. K., Woo, J.-H., Ban, S.-J., Lee, M.-D., Lim, C.-S., Park, M.-K., Shin, H. J., Cho, S., Peterson, D., and Song, C.-K.: Impacts of local vs. trans-boundary emissions from different sectors on PM<sub>2.5</sub> exposure in South Korea during the KORUS-AQ campaign, *Atmos. Environ.*, 203, 196–205, <https://doi.org/10.1016/j.atmosenv.2019.02.008>, 2019.
- 680 Chong, H., Lee, H., Koo, J.-H., Kim, J., Jeong, U., Kim, W., Kim, S.-W., Herman, J. R., Abuhassan, N. K., Ahn, J.-Y., Park, J.-H., Kim, S.-K., Moon, K.-J., Choi, W.-J., and Park, S. S.: Regional Characteristics of NO<sub>2</sub> Column Densities from Pandora Observations during the MAPS-Seoul Campaign, *Aerosol Air Qual. Res.*, 18, 2207–2219, <https://doi.org/10.4209/aaqr.2017.09.0341>, 2018.
- 685 Coggon, M. M., Gkatzelis, G. I., McDonald, B. C., Gilman, J. B., Schwantes, R. H., Abuhassan, N., Aikin, K. C., Arend, M. F., Berkoff, T. A., Brown, S. S., Campos, T. L., Dickerson, R. R., Gronoff, G., Hurley, J. F., Isaacman-VanWertz, G., Koss, A. R., Li, M., McKeen, S. A., Moshary, F., Peischl, J., Pospisilova, V., Ren, X., Wilson, A., Wu, Y., Trainer, M., and Warneke, C.: Volatile chemical product emissions enhance ozone and modulate urban chemistry, *P. Natl. Acad. Sci. U.S.A.*, 118, e2026653118, <https://doi.org/10.1073/pnas.2026653118>, 2021.
- 690 Crawford, J. H., Ahn, J.-Y., Al-Saadi, J., Chang, L., Emmons, L. K., Kim, J., Lee, G., Park, J.-H., Park, R. J., Woo, J. H., Song, C.-K., Hong, J.-H., Hong, Y.-D., Lefer, B. L., Lee, M., Lee, T., Kim, S., Min, K.-E., Yum, S. S., Shin, H. J., Kim, Y.-W., Choi, J.-S., Park, J.-S., Szykman, J. J., Long, R. W., Jordan, C. E., Simpson, I. J., Fried, A., Dibb, J. E., Cho, S., and Kim, Y. P.: The Korea–United States Air Quality (KORUS-AQ) field study, *Elem. Sci. Anth.*, 9, 00163, <https://doi.org/10.1525/elementa.2020.00163>, 2021.
- 695 Crounse, J. D., McKinney, K. A., Kwan, A. J., and Wennberg, P. O.: Measurement of gas-phase hydroperoxides by chemical ionization mass spectrometry (CIMS), *Anal. Chem.*, 78, 6726–6732, <https://doi.org/10.1021/ac0604235>, 2006.
- Eskes, H. J. and Boersma, K. F.: Averaging kernels for DOAS total-column satellite retrievals, *Atmos. Chem. Phys.*, 7, 1285–1291, <https://doi.org/10.5194/acp-3-1285-2003>, 2003.
- Fairlie, T. D., Jacob, D. J., Dibb, J. E., Alexander, B., Avery, M. A., van Donkelaar, A., and Zhang, L.: Impact of mineral dust on nitrate, sulfate, and ozone in transpacific Asian pollution plumes, *Atmos. Chem. Phys.*, 10, 3999–4012, <https://doi.org/10.5194/acp-10-3999-2010>, 2010.
- 705 Faloona, I. C., Tan, D., Leshner, R. L., Hazen, N. L., Frame, C. L., Simpas, J. B., Harder, H., Martinez, M., Di Carlo, P., Ren, X., and Brune, W. H.: A Laser-induced Fluorescence Instrument for Detecting Tropospheric OH and HO<sub>2</sub>: Characteristics and Calibration, *J. Atmos. Chem.*, 47, 139–167, <https://doi.org/10.1023/B:JOCH.0000021036.53185.0e>, 2004.
- 710 Flynn, L., Long, C., Wu, X., Evans, R., Beck, C. T., Petropavlovskikh, I., McConville, G., Yu, W., Zhang, Z., Niu, J., Beach, E., Hao, Y., Pan, C., Sen, B., Novicki, M., Zhou, S., and Seftor, C.: Performance of the Ozone Mapping and Profiler Suite (OMPS) products, *J. Geophys. Res. Atmos.*, 119, 6181–6195, <https://doi.org/10.1002/2013JD020467>, 2014.
- DeCarlo, P. F., Kimmel, J. R., Trimborn, A., Northway, M. J., Jayne, J. T., Aiken, A. C., Gonin, M., Fuhrer, K., Horvath, T., Docherty, K. S., Worsnop, D. R., and Jimenez, J. L.: Field-Deployable, High-Resolution, Time-of-Flight Aerosol Mass Spectrometer, *Anal. Chem.*, 78, 8281–8289, <https://doi.org/10.1021/ac061249n>, 2006.
- 715 de Foy, B., Lu, Z., Streets, D. G., Lamsal, L. N., and Duncan, B. N.: Estimates of power plant NO<sub>x</sub> emissions and lifetimes from OMI NO<sub>2</sub> satellite retrievals, *Atmos. Environ.*, 116, 1–11, <https://doi.org/10.1016/j.atmosenv.2015.05.056>, 2015.

- 720 Gaubert, B., Emmons, L. K., Raeder, K., Tilmes, S., Miyazaki, K., Arellano Jr., A. F., Elguindi, N., Granier, C., Tang, W., Barré, J., Worden, H. M., Buchholz, R. R., Edwards, D. P., Franke, P., Anderson, J. L., Saunio, M., Schroeder, J., Woo, J.-H., Simpson, I. J., Blake, D. R., Meinardi, S., Wennberg, P. O., Crouse, J., Teng, A., Kim, M., Dickerson, R. R., He, H., Ren, X., Pusede, S. E., and Diskin, G. S.: Correcting model biases of CO in East Asia: impact on oxidant distributions during KORUS-AQ, *Atmos. Chem. Phys.*, 20, 14617–14647, <https://doi.org/10.5194/acp-20-14617-2020>, 2020.
- 725 Goldberg, D. L., Saide, P. E., Lamsal, L. N., de Foy, B., Lu, Z., Woo, J.-H., Kim, Y., Kim, J., Gao, M., Carmichael, G., and Streets, D. G.: A top-down assessment using OMI NO<sub>2</sub> suggests an underestimate in the NO<sub>x</sub> emissions inventory in Seoul, South Korea, during KORUS-AQ, *Atmos. Chem. Phys.*, 19, 1801–1818, <https://doi.org/10.5194/acp-19-1801-2019>, 2019.
- 730 Guenther, A. B., Jiang, X., Heald, C. L., Sakulyanontvittaya, T., Duhl, T., Emmons, L. K., and Wang, X.: The Model of Emissions of Gases and Aerosols from Nature version 2.1 (MEGAN2.1): an extended and updated framework for modeling biogenic emissions, *Geosci. Model Dev.*, 5, 1471–1492, <https://doi.org/10.5194/gmd-5-1471-2012>, 2012.
- 735 Heim, E. W., Dibb, J., Scheuer, E., Jost, P. C., Nault, B. A., Jimenez, J. L., Peterson, D., Knute, C., Fenn, M., Hair, J., Beyersdorf, A. J., Corr, C., and Anderson, B. E.: Asian dust observed during KORUS-AQ facilitates the uptake and incorporation of soluble pollutants during transport to South Korea, *Atmos. Environ.*, 224, 117305, <https://doi.org/10.1016/j.atmosenv.2020.117305>, 2020.
- 740 Holmes, C. D., Bertram, T. H., Confer, K. L., Graham, K. A., Ronan, A. C., Wirks, C. K., and Shah, V.: The Role of Clouds in the Tropospheric NO<sub>x</sub> Cycle: A New Modeling Approach for Cloud Chemistry and Its Global Implications, *Geophys. Res. Lett.*, 46, 4980–4990, <https://doi.org/10.1029/2019GL081990>, 2019.
- Hudman, R. C., Moore, N. E., Mebust, A. K., Martin, R. V., Russell, A. R., Valin, L. C., and Cohen, R. C.: Steps towards a mechanistic model of global soil nitric oxide emissions: implementation and space based-constraints, *Atmos. Chem. Phys.*, 12, 7779–7795, <https://doi.org/10.5194/acp-12-7779-2012>, 2012.
- 745 Huijnen, V., Williams, J., van Weele, M., van Noije, T., Krol, M., Dentener, F., Segers, A., Houweling, S., Peters, W., de Laat, J., Boersma, F., Bergamaschi, P., van Velthoven, P., Le Sager, P., Eskes, H., Alkemade, F., Scheele, R., Nédélec, P., and Pätz, H.-W.: The global chemistry transport model TM5: description and evaluation of the tropospheric chemistry version 3.0, *Geosci. Model Dev.*, 3, 445–473, <https://doi.org/10.5194/gmd-3-445-2010>, 2010.
- 750 Jaeglé, L., Quinn, P. K., Bates, T. S., Alexander, B., and Lin, J.-T.: Global distribution of sea salt aerosols: new constraints from in situ and remote sensing observations, *Atmos. Chem. Phys.*, 11, 3137–3157, <https://doi.org/10.5194/acp-11-3137-2011>, 2011.
- 755 Jordan, C. E., Crawford, J. H., Beyersdorf, A. J., Eck, T. F., Halliday, H. S., Nault, B. A., Chang, L.-S., Park, J., Park, R., Lee, G., Kim, H., Ahn, J., Cho, S., Shin, H. J., Lee, J. H., Jung, J., Kim, D.-S., Lee, M., Lee, T., Whitehill, A., Szykman, J., Schueneman, M. K., Campuzano-Jost, P., Jimenez, J. L., DiGangi, J. P., Diskin, G. S., Anderson, B. E., Moore, R. H., Ziemba, L. D., Fenn, M. A., Hair, J. W., Kuehn, R. E., Holz, R. E., Chen, G., Travis, K., Shook, M., Peterson, D. A., Lamb, K. D., and Schwarz, J. P.: Investigation of factors controlling PM<sub>2.5</sub> variability across the South Korean Peninsula during KORUS-AQ, *Elem. Sci. Anth.*, 8, 28, <https://doi.org/10.1525/elementa.424>, 2020.
- 760 Kasibhatla, P., Sherwen, T., Evans, M. J., Carpenter, L. J., Reed, C., Alexander, B., Chen, Q., Sulprizio, M. P., Lee, J. D., Read, K. A., Bloss, W., Crilley, L. R., Keene, W. C., Pszenny, A. A. P., and Hodzic, A.: Global impact of nitrate photolysis in sea-salt aerosol on NO<sub>x</sub>, OH, and O<sub>3</sub>; in the marine boundary layer, *Atmos. Chem. Phys.*, 18, 11185–11203, <https://doi.org/10.5194/acp-18-11185-2018>, 2018.

- 765 Kim, H., Zhang, Q., and Heo, J.: Influence of intense secondary aerosol formation and long-range transport on aerosol chemistry and properties in the Seoul Metropolitan Area during spring time: results from KORUS-AQ, *Atmos. Chem. Phys.*, 18, 7149–7168, <https://doi.org/10.5194/acp-18-7149-2018>, 2018.
- Kim, H., Park, R. J., Kim, S., Brune, W. H., Diskin, G. S., Fried, A., Hall, S. R., Weinheimer, A. J., Wennberg, P., Wisthaler, A., Blake, D. R., and Ullmann, K.: Observed versus simulated OH reactivity during  
770 KORUS-AQ campaign: Implications for emission inventory and chemical environment in East Asia, *Elem. Sci. Anth.*, 10, 00030, <https://doi.org/10.1525/elementa.2022.00030>, 2022.
- Kim, J., Jeong, U., Ahn, M.-H., Kim, J. H., Park, R. J., Lee, H., Song, C. H., Choi, Y.-S., Lee, K.-H., Yoo, J.-M., Jeong, M.-J., Park, S. K., Lee, K.-M., Song, C.-K., Kim, S.-W., Kim, Y. J., Kim, S.-W., Kim, M., Go, S., Liu, X., Chance, K., Chan Miller, C., Al-Saadi, J., Veihelmann, B., Bhartia, P. K., Torres,  
775 O., Abad, G. G., Haffner, D. P., Ko, D. H., Lee, S. H., Woo, J.-H., Chong, H., Park, S. S., Nicks, D., Choi, W. J., Moon, K.-J., Cho, A., Yoon, J., Kim, S., Hong, H., Lee, K., Lee, H., Lee, S., Choi, M., Veeffkind, P., Levelt, P. F., Edwards, D. P., Kang, M., Eo, M., Bak, J., Baek, K., Kwon, H.-A., Yang, J., Park, J., Han, K. M., Kim, B.-R., Shin, H.-W., Choi, H., Lee, E., Chong, J., Cha, Y., Koo, J.-H., Irie, H., Hayashida, S., Kasai, Y., Kanaya, Y., Liu, C., Lin, J., Crawford, J. H., Carmichael, G. R.,  
780 Newchurch, M. J., Lefer, B. L., Herman, J. R., Swap, R. J., Lau, A. K. H., Kurosu, T. P., Jaross, G., Ahlers, B., Dobber, M., McElroy, C. T., and Choi, Y.: New Era of Air Quality Monitoring from Space: Geostationary Environment Monitoring Spectrometer (GEMS), *B. Am. Meteorol. Soc.*, 101, E1–E22, <https://doi.org/10.1175/BAMS-D-18-0013.1>, 2020.
- Kim, S., Sanchez, D., Wang, M., Seco, R., Jeong, D., Hughes, S., Barletta, B., Blake, D. R., Jung, J., Kim, D., Lee, G., Lee, M., Ahn, J., Lee, S.-D., Cho, G., Sung, M.-Y., Lee, Y.-H., Kim, D. B., Kim, Y.,  
785 Woo, J.-H., Jo, D., Park, R., Park, J.-H., Hong, Y.-D., and Hong, J.-H.: OH reactivity in urban and suburban regions in Seoul, South Korea – an East Asian megacity in a rapid transition, *Faraday Discuss.*, 189, 231–251, <https://doi.org/10.1039/C5FD00230C>, 2016.
- Kleipool, Q. L., Dobber, M. R., de Haan, J. F., and Levelt, P. F.: Earth surface reflectance climatology from  
790 3 years of OMI data, *J. Geophys. Res.*, 113, D18308, <https://doi.org/10.1029/2008JD010290>, 2008.
- KORUS-AQ Science Team: KORUS-AQ Data, NASA Langley Research Center, <https://doi.org/10.5067/Suborbital/KORUSAQ/DATA01>, 2019.
- Kwon, H.-A., Park, R. J., Oak, Y. J., Nowlan, C. R., Janz, S. J., Kowalewski, M. G., Fried, A., Walega, J.,  
795 Bates, K. H., Choi, J., Blake, D. R., Wisthaler, A., and Woo, J.-H.: Top-down estimates of anthropogenic VOC emissions in South Korea using formaldehyde vertical column densities from aircraft during the KORUS-AQ campaign, *Elem. Sci. Anth.*, 9, 00109, <https://doi.org/10.1525/elementa.2021.00109>, 2021.
- Lakey, P. S. J., George, I. J., Whalley, L. K., Baeza-Romero, M. T., and Heard, D. E.: Measurements of the  
800 HO<sub>2</sub> Uptake Coefficients onto Single Component Organic Aerosols, *Environ. Sci. Technol.*, 49, 4878–4885, <https://doi.org/10.1021/acs.est.5b00948>, 2015.
- Lamsal, L. N., Krotkov, N. A., Vasilkov, A., Marchenko, S., Qin, W., Yang, E.-S., Fasnacht, Z., Joiner, J.,  
Choi, S., Haffner, D., Swartz, W. H., Fisher, B., and Bucsele, E.: Ozone Monitoring Instrument (OMI) Aura nitrogen dioxide standard product version 4.0 with improved surface and cloud treatments, *Atmos. Meas. Tech.*, 14, 455–479, <https://doi.org/10.5194/amt-14-455-2021>, 2021.
- 805 Laughner, J. L. and Cohen, R. C.: Direct observation of changing NO<sub>x</sub> lifetime in North American cities, *Science*, 366, 723–727, <https://doi.org/10.1126/science.aax6832>, 2019.
- Lee, H., Park, J., and Hong, H.: Geostationary Environment Monitoring Spectrometer (GEMS) NO<sub>2</sub> retrieval Algorithm Theoretical Basis Document (ATBD) Version 1.0., National Institute of Environmental Research, South Korea, 2020.

- 810 Levelt, P. F., Joiner, J., Tamminen, J., Veeffkind, J. P., Bhartia, P. K., Stein Zweers, D. C., Duncan, B. N., Streets, D. G., Eskes, H., van der A, R., McLinden, C., Fioletov, V., Carn, S., de Laat, J., DeLand, M., Marchenko, S., McPeters, R., Ziemke, J., Fu, D., Liu, X., Pickering, K., Apituley, A., González Abad, G., Arola, A., Boersma, F., Chan Miller, C., Chance, K., de Graaf, M., Hakkarainen, J., Hassinen, S., Ialongo, I., Kleipool, Q., Krotkov, N., Li, C., Lamsal, L., Newman, P., Nowlan, C.,
- 815 Suleiman, R., Tilstra, L. G., Torres, O., Wang, H., and Wargan, K.: The Ozone Monitoring Instrument: overview of 14 years in space, *Atmos. Chem. Phys.*, 18, 5699–5745, <https://doi.org/10.5194/acp-18-5699-2018>, 2018.
- Lin, H., Jacob, D. J., Lundgren, E. W., Sulprizio, M. P., Keller, C. A., Fritz, T. M., Eastham, S. D., Emmons, L. K., Campbell, P. C., Baker, B., Saylor, R. D., and Montuoro, R.: Harmonized Emissions Component (HEMCO) 3.0 as a versatile emissions component for atmospheric models: application in the GEOS-Chem, NASA GEOS, WRF-GC, CESM2, NOAA GEFS-Aerosol, and NOAA UFS models, *Geosci. Model Dev.*, 14, 5487–5506, <https://doi.org/10.5194/gmd-14-5487-2021>, 2021.
- 820 Lin, J. T., McElroy, M. B., and Boersma, K. F.: Constraint of anthropogenic NO<sub>x</sub> emissions in China from different sectors: a new methodology using multiple satellite retrievals, *Atmos. Chem. and Phys.*, 10, 63–78, <https://doi.org/10.5194/acp-10-63-2010>, 2010.
- 825 Lin, J. T., Liu, Z., Zhang, Q., Liu, H., Mao, J., and Zhuang, G.: Modeling uncertainties for tropospheric nitrogen dioxide columns affecting satellite-based inverse modeling of nitrogen oxides emissions, *Atmos. Chem. Phys.*, 12, 12255–12275, <https://doi.org/10.5194/acp-12-12255-2012>, 2012.
- Mao, J., Ren, X., Brune, W. H., Olson, J. R., Crawford, J. H., Fried, A., Huey, L. G., Cohen, R. C., Heikes, B., Singh, H. B., Blake, D. R., Sachse, G. W., Diskin, G. S., Hall, S. R., and Shetter, R. E.: Airborne measurement of OH reactivity during INTEX-B, *Atmos. Chem. Phys.*, 11, 163–173, <https://doi.org/10.5194/acp-9-163-2009>, 2009.
- 830 Mao, J., Jacob, D. J., Evans, M. J., Olson, J. R., Ren, X., Brune, W. H., Clair, J. M. St., Crouse, J. D., Spencer, K. M., Beaver, M. R., Wennberg, P. O., Cubison, M. J., Jimenez, J. L., Fried, A., Weibring, P., Walega, J. G., Hall, S. R., Weinheimer, A. J., Cohen, R. C., Chen, G., Crawford, J. H., McNaughton, C., Clarke, A. D., Jaeglé, L., Fisher, J. A., Yantosca, R. M., Le Sager, P., and Carouge, C.: Chemistry of hydrogen oxide radicals (HO<sub>x</sub>) in the Arctic troposphere in spring, *Atmos. Chem. Phys.*, 10, 5823–5838, <https://doi.org/10.5194/acp-10-5823-2010>, 2010.
- 835 Mao, J., Fan, S., Jacob, D. J., and Travis, K. R.: Radical loss in the atmosphere from Cu-Fe redox coupling in aerosols, *Atmos. Chem. Phys.*, 13, 509–519, <https://doi.org/10.5194/acp-13-509-2013>, 2013.
- Martin, R. V., Chance, K., Jacob, D. J., Kurosu, T. P., Spurr, R. J. D., Bucsel, E., Gleason, J. J., Palmer, P. I., Bey, I., Fiore, A. M., Li, Q., Yantosca, R. M., and Koelmeijer, R. B. A.: An improved retrieval of tropospheric nitrogen dioxide from GOME, *J. Geophys. Res.*, 107, 4437, <https://doi.org/10.1029/2001JD001027>, 2002.
- 845 Martin, R. V., Jacob, D. J., Yantosca, R. M., Chin, M., and Ginoux, P.: Global and regional decreases in tropospheric oxidants from photochemical effects of aerosols, *J. Geophys. Res.*, 108, <https://doi.org/10.1029/2002JD002622>, 2003.
- McDonald, B. C., de Gouw, J. A., Gilman, J. B., Jathar, S. H., Akherati, A., Cappa, C. D., Jimenez, J. L., Lee-Taylor, J., Hayes, P. L., McKeen, S. A., Cui, Y. Y., Kim, S.-W., Gentner, D. R., Isaacman-VanWertz, G., Goldstein, A. H., Harley, R. A., Frost, G. J., Roberts, J. M., Ryerson, T. B., and Trainer, M.: Volatile chemical products emerging as largest petrochemical source of urban organic emissions, *Science*, 359, 760–764, <https://doi.org/10.1126/science.aag0524>, 2018.
- 850 McDuffie, E. E., Martin, R. V., Spadaro, J. V., Burnett, R., Smith, S. J., O'Rourke, P., Hammer, M. S., van Donkelaar, A., Bindle, L., Shah, V., Jaeglé, L., Luo, G., Yu, F., Adeniran, J. A., Lin, J., and Brauer,

- 855 M.: Source sector and fuel contributions to ambient PM<sub>2.5</sub> and attributable mortality across multiple spatial scales, *Nat. Commun.*, 12, 3594, <https://doi.org/10.1038/s41467-021-23853-y>, 2021.
- Miyazaki, K., Sekiya, T., Fu, D., Bowman, K. W., Kulawik, S. S., Sudo, K., Walker, T., Kanaya, Y., Takigawa, M., Ogochi, K., Eskes, H., Boersma, K. F., Thompson, A. M., Gaubert, B., Barre, J., and Emmons, L. K.: Balance of Emission and Dynamical Controls on Ozone During the Korea-United States Air Quality Campaign From Multiconstituent Satellite Data Assimilation, *J. Geophys. Res.-Atmos.*, 124, 387–413, <https://doi.org/10.1029/2018JD028912>, 2019.
- 860 Murray, L. T., Jacob, D. J., Logan, J. A., Hudman, R. C., and Koshak, W. J.: Optimized regional and interannual variability of lightning in a global chemical transport model constrained by LIS/OTD satellite data, *J. Geophys. Res.*, 117, <https://doi.org/10.1029/2012JD017934>, 2012.
- 865 [Naik, V., Voulgarakis, A., Fiore, A. M., Horowitz, L. W., Lamarque, J.-F., Lin, M., Prather, M. J., Young, P. J., Bergmann, D., Cameron-Smith, P. J., Cionni, I., Collins, W. J., Dalsøren, S. B., Doherty, R., Eyring, V., Faluvegi, G., Folberth, G. A., Josse, B., Lee, Y. H., MacKenzie, I. A., Nagashima, T., van Noije, T. P. C., Plummer, D. A., Righi, M., Rumbold, S. T., Skeie, R., Shindell, D. T., Stevenson, D. S., Strode, S., Sudo, K., Szopa, S., and Zeng, G.: Preindustrial to present-day changes in tropospheric hydroxyl radical and methane lifetime from the Atmospheric Chemistry and Climate Model Intercomparison Project \(ACCMIP\), \*Atmos. Chem. Phys.\*, 13, 5277–5298, <https://doi.org/10.5194/acp-13-5277-2013>, 2013.](#)
- [NASA: Airborne and Satellite Investigation of Asian Air Quality \(ASIA-AQ\) White Paper, NASA Earth Science Project Office.](#)
- 875 [https://espo.nasa.gov/sites/default/files/documents/Draft%20Planning%20Document%20for%20ASIA-AQ\\_20210802.pdf](https://espo.nasa.gov/sites/default/files/documents/Draft%20Planning%20Document%20for%20ASIA-AQ_20210802.pdf), 2021.
- Nault, B. A., Garland, C., Pusede, S. E., Wooldridge, P. J., Ullmann, K., Hall, S. R., and Cohen, R. C.: Measurements of CH<sub>3</sub>O<sub>2</sub>NO<sub>2</sub> in the upper troposphere, *Atmos. Meas. Tech.*, 8, 987–997, <https://doi.org/10.5194/amt-8-987-2015>, 2015.
- 880 Nault, B. A., Campuzano-Jost, P., Day, D. A., Schroder, J. C., Anderson, B., Beyersdorf, A. J., Blake, D. R., Brune, W. H., Choi, Y., Corr, C. A., de Gouw, J. A., Dibb, J., DiGangi, J. P., Diskin, G. S., Fried, A., Huey, L. G., Kim, M. J., Knote, C. J., Lamb, K. D., Lee, T., Park, T., Pusede, S. E., Scheuer, E., Thornhill, K. L., Woo, J.-H., and Jimenez, J. L.: Secondary organic aerosol production from local emissions dominates the organic aerosol budget over Seoul, South Korea, during KORUS-AQ, *Atmos. Chem. Phys.*, 18, 17769–17800, <https://doi.org/10.5194/acp-18-17769-2018>, 2018.
- 885 Nussbaumer, C. M., Parchatka, U., Tadic, I., Bohn, B., Marno, D., Martinez, M., Rohloff, R., Harder, H., Kluge, F., Pfeilsticker, K., Obersteiner, F., Zöger, M., Doerich, R., Crowley, J. N., Lelieveld, J., and Fischer, H.: Modification of a conventional photolytic converter for improving aircraft measurements of NO<sub>2</sub> via chemiluminescence, *Atmos. Meas. Tech.*, 14, 6759–6776, <https://doi.org/10.5194/amt-14-6759-2021>, 2021.
- 890 Oak, Y. J., Park, R. J., Schroeder, J. R., Crawford, J. H., Blake, D. R., Weinheimer, A. J., Woo, J.-H., Kim, S.-W., Yeo, H., Fried, A., Wisthaler, A., and Brune, W. H.: Evaluation of simulated O<sub>3</sub> production efficiency during the KORUS-AQ campaign: Implications for anthropogenic NO<sub>x</sub> emissions in Korea, *Elem. Sci. Anth.*, 7, 56, <https://doi.org/10.1525/elementa.394>, 2019.
- 895 Palmer, P. I., Jacob, D. J., Chance, K., Martin, R. V., Spurr, R. J. D., Kurosu, T. P., Bey, I., Yantosca, R., Fiore, A., and Li, Q.: Air mass factor formulation for spectroscopic measurements from satellites: Application to formaldehyde retrievals from the Global Ozone Monitoring Experiment, *J. Geophys. Res.*, 106, 14539–14550, <https://doi.org/10.1029/2000JD900772>, 2001.
- 900 Park, J., Lee, H., Hong, H., Yang, J., van Roozendaal, M., Kim, S., Kim, J., Lee, D., Fayt, C., Ko, D. ho, Lee, S.-H., A. Krotkov, N., Wagner, T., Richter, A., and N. Lamsal, L.: First results of diurnal NO<sub>2</sub> column

Moved (insertion) [1]

Moved (insertion) [2]

Moved (insertion) [3]

Moved (insertion) [4]

Moved (insertion) [5]



variation over Asia from the Geostationary Environment Monitoring Spectrometer (GEMS), Copernicus Meetings, Vienna, Austria, 23-27 May 2022, EGU22-3280, <https://doi.org/10.5194/egusphere-egu22-3280>, 2022.

905 | Park, R. J., Oak, Y. J., Emmons, L. K., Kim, C.-H., Pfister, G. G., Carmichael, G. R., Saide, P. E., Cho, S.-Y., Kim, S., Woo, J.-H., Crawford, J. H., Gaubert, B., Lee, H.-J., Park, S.-Y., Jo, Y.-J., Gao, M., Tang, B., Stanier, C. O., Shin, S. S., Park, H. Y., Bae, C., and Kim, E.: Multi-model inter-comparisons of air quality simulations for the KORUS-AQ campaign, *Elem. Sci. Anth.*, 9, 00139, <https://doi.org/10.1525/elementa.2021.00139>, 2021.

910 | Penn, E. and Holloway, T.: Evaluating current satellite capability to observe diurnal change in nitrogen oxides in preparation for geostationary satellite missions, *Environ. Res. Lett.*, 15, 034038, <https://doi.org/10.1088/1748-9326/ab6b36>, 2020.

Qu, Z., Jacob, D. J., Silvern, R. F., Shah, V., Campbell, P. C., Valin, L. C., and Murray, L. T.: US COVID-19 Shutdown Demonstrates Importance of Background NO<sub>2</sub> in Inferring NO<sub>x</sub> Emissions from Satellite NO<sub>2</sub> Observations, *Geophys. Res. Lett.*, 48, <https://doi.org/10.1029/2021GL092783>, 2021.

915 | Reed, C., Evans, M. J., Di Carlo, P., Lee, J. D., and Carpenter, L. J.: Interferences in photolytic NO<sub>2</sub> measurements: explanation for an apparent missing oxidant?, *Atmos. Chem. Phys.*, 16, 4707–4724, <https://doi.org/10.5194/acp-16-4707-2016>, 2016.

920 | Reed, C., Evans, M. J., Crilley, L. R., Bloss, W. J., Sherwen, T., Read, K. A., Lee, J. D., and Carpenter, L. J.: Evidence for renoxification in the tropical marine boundary layer, *Atmos. Chem. Phys.*, 17, 4081–4092, <https://doi.org/10.5194/acp-17-4081-2017>, 2017.

925 | Richter, A., Burrows, J. P., Nüß, H., Granier, C., and Niemeier, U.: Increase in tropospheric nitrogen dioxide over China observed from space, *Nature*, 437, 129–132, <https://doi.org/10.1038/nature04092>, 2005.

Romer, P. S., Wooldridge, P. J., Crouse, J. D., Kim, M. J., Wennberg, P. O., Dibb, J. E., Scheuer, E., Blake, D. R., Meinardi, S., Brosius, A. L., Thames, A. B., Miller, D. O., Brune, W. H., Hall, S. R., Ryerson, T. B., and Cohen, R. C.: Constraints on Aerosol Nitrate Photolysis as a Potential Source of HONO and NO<sub>x</sub>, *Environ. Sci. Technol.*, 52, 13738–13746, <https://doi.org/10.1021/acs.est.8b03861>, 2018.

Sachse, G. W., Hill, G. F., Wade, L. O., and Perry, M. G.: Fast-response, high-precision carbon monoxide sensor using a tunable diode laser absorption technique, *J. Geophys. Res.*, 92, 2071, <https://doi.org/10.1029/JD092iD02p02071>, 1987.

930 | Schroeder, J. R., Crawford, J. H., Ahn, J.-Y., Chang, L., Fried, A., Walega, J., Weinheimer, A., Montzka, D. D., Hall, S. R., Ullmann, K., Wisthaler, A., Mikoviny, T., Chen, G., Blake, D. R., Blake, N. J., Hughes, S. C., Meinardi, S., Diskin, G., Digangi, J. P., Choi, Y., Pusede, S. E., Huey, G. L., Tanner, D. J., Kim, M., and Wennberg, P.: Observation-based modeling of ozone chemistry in the Seoul metropolitan area during the Korea-United States Air Quality Study (KORUS-AQ), *Elem. Sci. Anth.*, 8, 3, <https://doi.org/10.1525/elementa.400>, 2020.

935 | Shah, V., Jacob, D. J., Dang, R., Lamsal, L. N., Strode, S. A., Steenrod, S. D., Boersma, K. F., Eastham, S. D., Fritz, T. M., Thompson, C., Peischl, J., Bourgeois, I., Pollack, I. B., Nault, B. A., Cohen, R. C., Campuzano-Jost, P., Jimenez, J. L., Andersen, S. T., Carpenter, L. J., Sherwen, T., and Evans, M. J.: Nitrogen oxides in the free troposphere: [implications](#) for tropospheric oxidants and the interpretation of satellite NO<sub>2</sub> measurements, *Atmos. Chem. Phys.*, 23, 1227–1257, <https://doi.org/10.5194/acp-23-1227-2023>, 2023.

940 | Shindell, D. T., Faluvegi, G., Stevenson, D. S., Krol, M. C., Emmons, L. K., Lamarque, J.-F., Pétron, G., Dentener, F. J., Ellingsen, K., Schultz, M. G., Wild, O., Amann, M., Atherton, C. S., Bergmann, D. J., Bey, I., Butler, T., Cofala, J., Collins, W. J., Derwent, R. G., Doherty, R. M., Drevet, J., Eskes, H. J., Fiore, A. M., Gauss, M., Hauglustaine, D. A., Horowitz, L. W., Isaksen, I. S. A., Lawrence, M. G.,

Moved up [1]: . M.,

Moved up [2]: . J.,

Deleted: Jacob, D. J., Field, B. D., Yantosca, R

Deleted: and Chin, M.: Natural and transboundary pollution influences on sulfate-nitrate-ammonium aerosols in the United States: Implications for policy, *J. Geophys. Res.*, 20, <https://doi.org/10.1029/2003JD004473>, 2004, Park, R

Deleted: Remer, L. A., Mattoo, S., Levy, R. C., Heidinger, A., Pierce, R. B., and Chin, M.: Retrieving aerosol in a cloudy environment: aerosol product availability as a function of spatial resolution, *Atmos. Meas. Tech.*, 5, 1823–1840, <https://doi.org/10.5194/amt-5-1823-2012>, 2012.

Deleted: Implications

Deleted:

Deleted: EGU sphere [preprint],

Deleted: <https://doi.org/10.5194/egusphere-2022-656>, 21 Jul 2022

Formatted: Subscript



- 965 Montanaro, V., Müller, J.-F., Pitari, G., Prather, M. J., Pyle, J. A., Rast, S., Rodriguez, J. M., Sanderson, M. G., Savage, N. H., Strahan, S. E., Sudo, K., Szopa, S., Unger, N., van Noije, T. P. C., and Zeng, G.: Multimodel simulations of carbon monoxide: Comparison with observations and projected near-future changes, *J. Geophys. Res.*, 111, D19306, <https://doi.org/10.1029/2006JD007100>, 2006.
- 970 Silvern, R. F., Jacob, D. J., Travis, K. R., Sherwen, T., Evans, M. J., Cohen, R. C., Laughner, J. L., Hall, S. R., Ullmann, K., Crouse, J. D., Wennberg, P. O., Peischl, J., and Pollack, I. B.: Observed NO/NO<sub>2</sub> Ratios in the Upper Troposphere Imply Errors in NO-NO<sub>2</sub>-O<sub>3</sub> Cycling Kinetics or an Unaccounted NO<sub>x</sub> Reservoir, *Geophys. Res. Lett.*, 45, 4466–4474, <https://doi.org/10.1029/2018GL077728>, 2018.
- 975 Silvern, R. F., Jacob, D. J., Mickley, L. J., Sulprizio, M. P., Travis, K. R., Marais, E. A., Cohen, R. C., Laughner, J. L., Choi, S., Joiner, J., and Lamsal, L. N.: Using satellite observations of tropospheric NO<sub>2</sub> columns to infer long-term trends in US NO<sub>x</sub> emissions: the importance of accounting for the free tropospheric NO<sub>2</sub> background, *Atmos. Chem. Phys.*, 19, 8863–8878, <https://doi.org/10.5194/acp-19-8863-2019>, 2019.
- 980 Simpson, I. J., Blake, D. R., Blake, N. J., Meinardi, S., Barletta, B., Hughes, S. C., Fleming, L. T., Crawford, J. H., Diskin, G. S., Emmons, L. K., Fried, A., Guo, H., Peterson, D. A., Wisthaler, A., Woo, J.-H., Barré, J., Gaubert, B., Kim, J., Kim, M. J., Kim, Y., Knote, C., Mikoviny, T., Pusede, S. E., Schroeder, J. R., Wang, Y., Wennberg, P. O., and Zeng, L.: Characterization, sources and reactivity of volatile organic compounds (VOCs) in Seoul and surrounding regions during KORUS-AQ, *Elem. Sci. Anth.*, 8, 37, <https://doi.org/10.1525/elementa.434>, 2020.
- 985 Spinei, E., Whitehill, A., Fried, A., Tiefengraber, M., Knepp, T. N., Herndon, S., Herman, J. R., Müller, M., Abuhassan, N., Cede, A., Richter, D., Walega, J., Crawford, J., Szykman, J., Valin, L., Williams, D. J., Long, R., Swap, R. J., Lee, Y., Nowak, N., and Poche, B.: The first evaluation of formaldehyde column observations by improved Pandora spectrometers during the KORUS-AQ field study, *Atmos. Meas. Tech.*, 11, 4943–4961, <https://doi.org/10.5194/amt-11-4943-2018>, 2018.
- 990 Stavroukou, T., Müller, J.-F., Boersma, K. F., De Smedt, I., and van der A, R. J.: Assessing the distribution and growth rates of NO<sub>x</sub> emission sources by inverting a 10-year record of NO<sub>2</sub> satellite columns, *Geophys. Res. Lett.*, 35, <https://doi.org/10.1029/2008GL033521>, 2008.
- 995 Taketani, F., Kanaya, Y., Pochanart, P., Liu, Y., Li, J., Okuzawa, K., Kawamura, K., Wang, Z., and Akimoto, H.: Measurement of overall uptake coefficients for HO<sub>2</sub> radicals by aerosol particles sampled from ambient air at Mts. Tai and Mang (China), *Atmos. Chem. Phys.*, 12, 11907–11916, <https://doi.org/10.5194/acp-12-11907-2012>, 2012.
- Thornton, J. A., Wooldridge, P. J., and Cohen, R. C.: Atmospheric NO<sub>2</sub>: In Situ Laser-Induced Fluorescence Detection at Parts per Trillion Mixing Ratios, *Anal. Chem.*, 72, 528–539, <https://doi.org/10.1021/ac9908905>, 2000.
- 000 Travis, K. R., Jacob, D. J., Fisher, J. A., Kim, P. S., Marais, E. A., Zhu, L., Yu, K., Miller, C. C., Yantosca, R. M., Sulprizio, M. P., Thompson, A. M., Wennberg, P. O., Crouse, J. D., St. Clair, J. M., Cohen, R. C., Laughner, J. L., Dibb, J. E., Hall, S. R., Ullmann, K., Wolfe, G. M., Pollack, I. B., Peischl, J., Neuman, J. A., and Zhou, X.: Why do models overestimate surface ozone in the Southeast United States?, *Atmos. Chem. Phys.*, 16, 13561–13577, <https://doi.org/10.5194/acp-16-13561-2016>, 2016.
- 005 Travis, K. R., Crawford, J. H., Chen, G., Jordan, C. E., Nault, B. A., Kim, H., Jimenez, J. L., Campuzano-Jost, P., Dibb, J. E., Woo, J.-H., Kim, Y., Zhai, S., Wang, X., McDuffie, E. E., Luo, G., Yu, F., Kim, S., Simpson, I. J., Blake, D. R., Chang, L., and Kim, M. J.: Limitations in representation of physical processes prevent successful simulation of PM<sub>2.5</sub>; during KORUS-AQ, *Atmos. Chem. Phys.*, 22, 7933–7958, <https://doi.org/10.5194/acp-22-7933-2022>, 2022.

010 Veefkind, J. P., Aben, I., McMullan, K., Förster, H., de Vries, J., Otter, G., Claas, J., Eskes, H. J., de Haan, J. F., Kleipool, Q., van Weele, M., Hasekamp, O., Hoogeveen, R., Landgraf, J., Snel, R., Tol, P., Ingmann, P., Voors, R., Kruizinga, B., Vink, R., Visser, H., and Levelt, P. F.: TROPOMI on the ESA Sentinel-5 Precursor: A GMES mission for global observations of the atmospheric composition for climate, air quality and ozone layer applications, *Remote Sens. Environ.*, 120, 70–83, <https://doi.org/10.1016/j.rse.2011.09.027>, 2012.

015 Walega, J. G., Dye, J. E., Grahek, F. E., and Ridley, B. K.: Compact measurement system for the simultaneous determination of NO, NO<sub>2</sub>, NO<sub>y</sub>, and O<sub>3</sub> using a small aircraft, in: *Measurement of Atmospheric Gases*, P. Soc. Photo-opt. Ins., 232–241, <https://doi.org/10.1117/12.46167>, 1991.

020 Wang, X., Jacob, D. J., Downs, W., Zhai, S., Zhu, L., Shah, V., Holmes, C. D., Sherwen, T., Alexander, B., Evans, M. J., Eastham, S. D., Neuman, J. A., Veres, P. R., Koenig, T. K., Volkamer, R., Huey, L. G., Bannan, T. J., Percival, C. J., Lee, B. H., and Thornton, J. A.: Global tropospheric halogen (Cl, Br, I) chemistry and its impact on oxidants, *Atmos. Chem. Phys.*, 21, 13973–13996, <https://doi.org/10.5194/acp-21-13973-2021>, 2021.

025 Woo, J.-H., Kim, Y., Kim, H.-K., Choi, K.-C., Eum, J.-H., Lee, J.-B., Lim, J.-H., Kim, J., and Seong, M.: Development of the CREATE Inventory in Support of Integrated Climate and Air Quality Modeling for Asia, *Sustainability*, 12, 7930, <https://doi.org/10.3390/su12197930>, 2020.

Ye, C., Zhou, X., Pu, D., Stutz, J., Festa, J., Spolaor, M., Tsai, C., Cantrell, C., Mauldin, R. L., Campos, T., Weinheimer, A., Hornbrook, R. S., Apel, E. C., Guenther, A., Kaser, L., Yuan, B., Karl, T., Haggerty, J., Hall, S., Ullmann, K., Smith, J. N., Ortega, J., and Knote, C.: Rapid cycling of reactive nitrogen in the marine boundary layer, *Nature*, 532, 489–491, <https://doi.org/10.1038/nature17195>, 2016.

030 Zhai, S., Jacob, D. J., Brewer, J. F., Li, K., Moch, J. M., Kim, J., Lee, S., Lim, H., Lee, H. C., Kuk, S. K., Park, R. J., Jeong, J. I., Wang, X., Liu, P., Luo, G., Yu, F., Meng, J., Martin, R. V., Travis, K. R., Hair, J. W., Anderson, B. E., Dibb, J. E., Jimenez, J. L., Campuzano-Jost, P., Nault, B. A., Woo, J.-H., Kim, Y., Zhang, Q., and Liao, H.: Relating geostationary satellite measurements of aerosol optical depth (AOD) over East Asia to fine particulate matter (PM<sub>2.5</sub>): insights from the KORUS-AQ aircraft campaign and GEOS-Chem model simulations, *Atmos. Chem. Phys.*, 21, 16775–16791, <https://doi.org/10.5194/acp-21-16775-2021>, 2021.

035 Zhai, S.: *Factors Controlling Peroxyacetyl Nitrate (PAN) in Polluted and Remote Atmospheres: Insights from the KORUS-AQ and ATom Campaigns*, American Meteorological Society (AMS) 102<sup>nd</sup> Annual Meeting, Houston, Texas, 23–27 January 2022, [https://acmg.seas.harvard.edu/files/acmg/files/shixian\\_ams2022\\_pan.pdf](https://acmg.seas.harvard.edu/files/acmg/files/shixian_ams2022_pan.pdf), 2022.

040 Zhai, S., Jacob, D. J., Pendergrass, D. C., Colombi, N. K., Shah, V., Yang, L. H., Zhang, Q., Wang, S., Kim, H., Sun, Y., Choi, J.-S., Park, J.-S., Luo, G., Yu, F., Woo, J.-H., Kim, Y., Dibb, J. E., Lee, T., Han, J.-S., Anderson, B. E., Li, K., and Liao, H.: Coarse particulate matter air quality in East Asia: implications for fine particulate nitrate, *EGU sphere [preprint]*, <https://doi.org/10.5194/egusphere-2022-1485>, 2023.

045 Zhang, C., Liu, C., Wang, Y., Si, F., Zhou, H., Zhao, M., Su, W., Zhang, W., Chan, K. L., Liu, X., Xie, P., Liu, J., and Wagner, T.: Preflight Evaluation of the Performance of the Chinese Environmental Trace Gas Monitoring Instrument (EMI) by Spectral Analyses of Nitrogen Dioxide, *IEEE Geosci. Remote S.*, 56, 3323–3332, <https://doi.org/10.1109/TGRS.2018.2798038>, 2018.

050 Zheng, B., Tong, D., Li, M., Liu, F., Hong, C., Geng, G., Li, H., Li, X., Peng, L., Qi, J., Yan, L., Zhang, Y., Zhao, H., Zheng, Y., He, K., and Zhang, Q.: Trends in China’s anthropogenic emissions since 2010 as the consequence of clean air actions, *Atmos. Chem. and Phys.*, 18, 14095–14111, <https://doi.org/10.5194/acp-18-14095-2018>, 2018.

Moved up [3]: . J.,

Moved up [4]: . H.,

Moved up [5]: Chem.

Deleted: Eastham, S. D., Sulprizio, M. P., Zhu, L., Chen, Q., Alexander, B., Sherwen, T., Evans, M

Deleted: Lee, B

Deleted: Haskins, J. D., Lopez-Hilfiker, F. D., Thornton, J. A., Huey, G. L., and Liao, H.: The role of chlorine in global tropospheric chemistry, *Atmos.*

Deleted: Phys., 19, 3981–4003, <https://doi.org/10.5194/acp-19-3981-2019>, 2019. Wang, X., Jacob, D. J.,

Moved down [6]: ., Jacob, D. J.,

Moved down [7]: Shah, V., Yang, L. H., Zhang, Q.,

Moved down [8]: Sun, Y.,

Moved down [9]: S., Luo, G., Yu, F., Woo, J.-H.,

Moved down [10]: ., Lee, T., Han, J.-S

Moved down [11]: ., Li, K., and Liao, H.: Coarse particulate matter air quality in East Asia: implications for fine particulate nitrate,

Deleted: Wang,

Deleted: Kim, Y., Kim, H

Deleted: arXiv [preprint], <https://arxiv.org/abs/2207.03625>, 8 July 2022a. Zhai, S

Deleted: 2022b

Moved (insertion) [6]

Moved (insertion) [7]

Moved (insertion) [8]

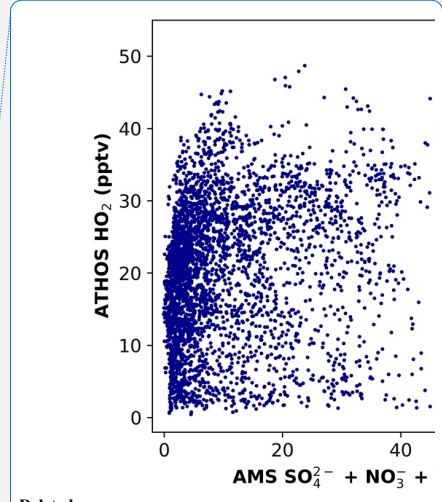
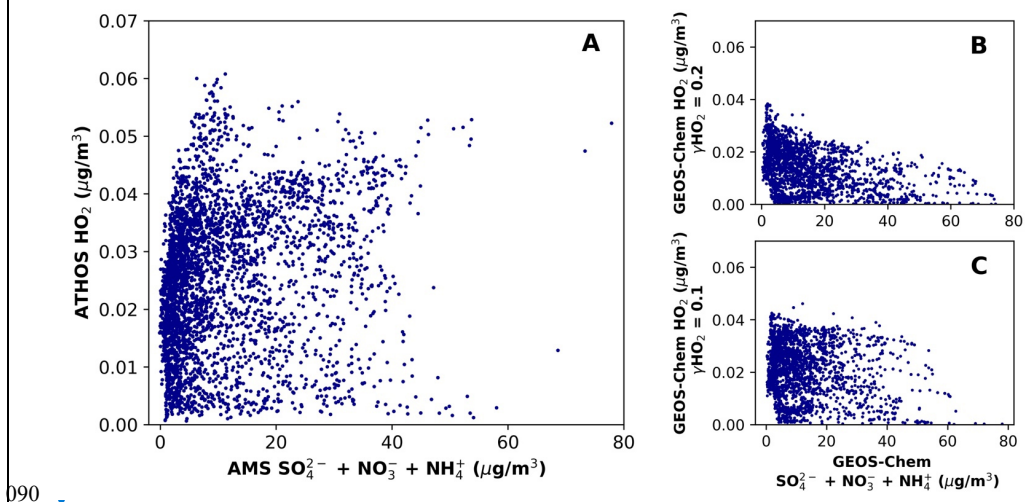
Moved (insertion) [9]

Moved (insertion) [10]

Moved (insertion) [11]

Zhou, X., Davis, A. J., Kieber, D. J., Keene, W. C., Maben, J. R., Maring, H., Dahl, E. E., Izaguirre, M. A., Sander, R., and Smoydzy, L.: Photochemical production of hydroxyl radical and hydroperoxides in water extracts of nascent marine aerosols produced by bursting bubbles from Sargasso seawater, *Geophys. Res. Lett.*, 35, L20803, <https://doi.org/10.1029/2008GL035418>, 2008.

085 Zou, Q., Song, H., Tang, M., and Lu, K.: Measurements of HO<sub>2</sub> uptake coefficient on aqueous (NH<sub>4</sub>)<sub>2</sub>SO<sub>4</sub> aerosol using aerosol flow tube with LIF system, *Chinese Chem. Lett.*, 30, 2236–2240, <https://doi.org/10.1016/j.ccllet.2019.07.041>, 2019.



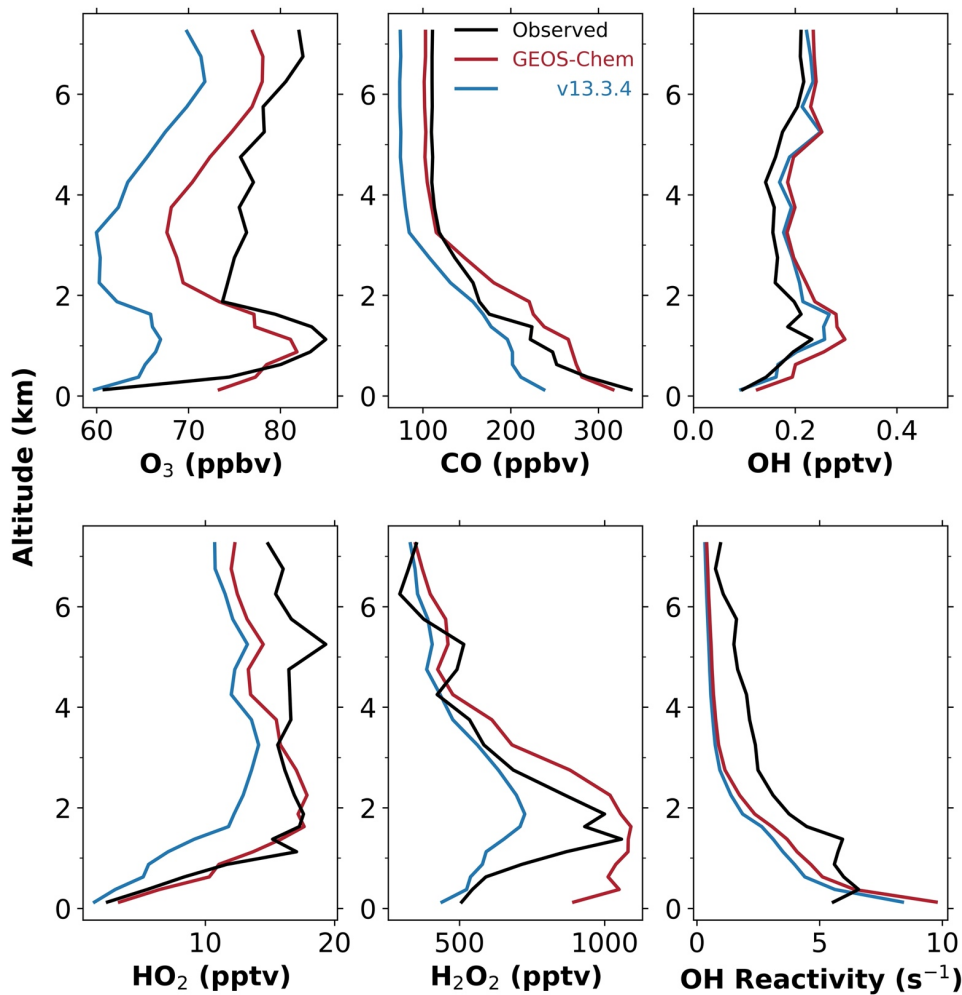
Deleted:

Deleted: The left panel

Deleted: top

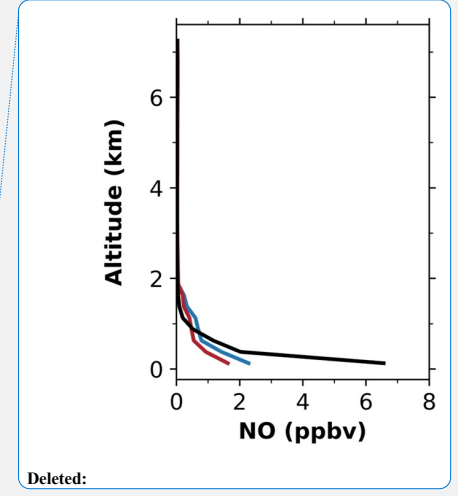
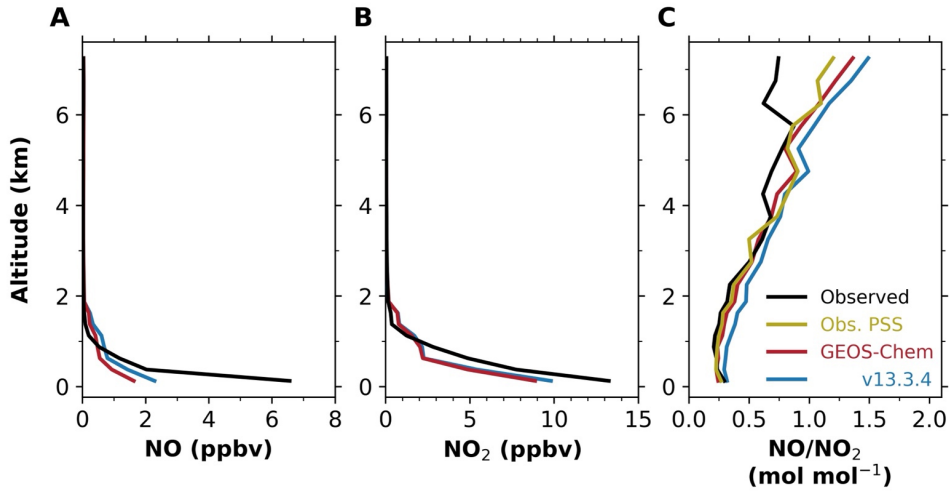
Deleted: bottom

090  
 095  
**Figure 1.** Relationship of HO<sub>2</sub> and sulfate-nitrate-ammonium (SNA) aerosol concentrations below 2km altitude during KORUS-AQ. **Panel A** shows the ensemble of observations from the ATHOS and AMS instruments. The right panels show GEOS-Chem model results with HO<sub>2</sub> reactive uptake coefficients ( $\gamma_{\text{HO}_2}$ ) of 0.2 (**panel B**) and 0.1 (**panel C**).



100 **Figure 2.** Median vertical profiles of species concentrations and OH reactivity (OHR) in the Seoul  
 Metropolitan Area (SMA; 37 – 37.6°N, 126.6 – 127.7°E) during KORUS-AQ. Observations are compared  
 to our GEOS-Chem simulation and to standard version 13.3.4 of the model. [Here and in the following Figures,](#)  
 105 [vertical profiles are constructed by binning the data in 0.25-km vertical intervals below 2 km altitude and 1-](#)  
[km vertical intervals above 2 km altitude.](#)

Deleted: the  
 Deleted:



Deleted:

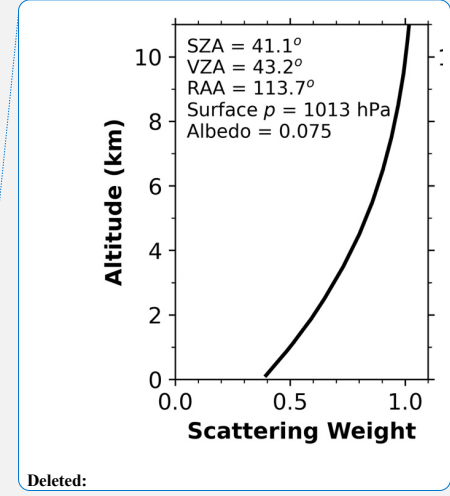
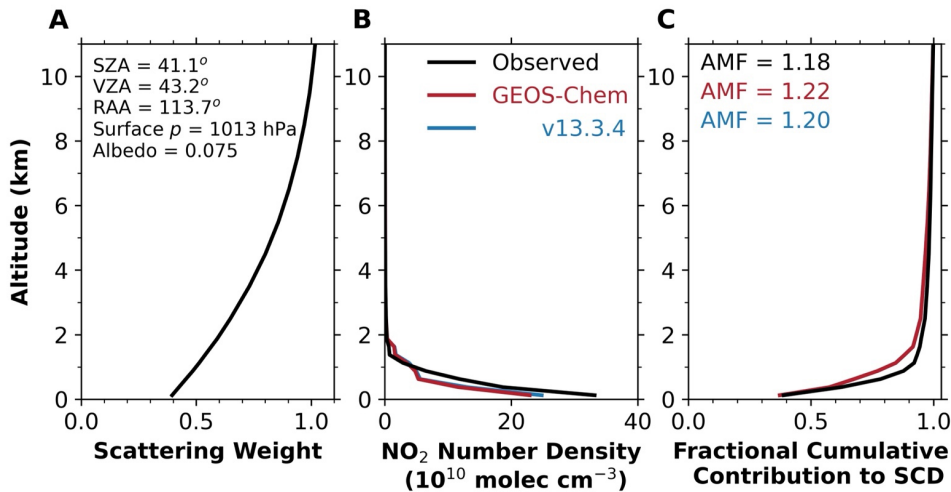
Deleted: ,

Deleted: ,

Deleted: is

110 **Figure 3.** Median vertical profiles of NO and NO<sub>2</sub> concentrations (panels A and B), and NO/NO<sub>2</sub>  
 concentration ratios (panel C), in the SMA (37 – 37.6°N, 126.6 – 127.7°E) during the KORUS-AQ campaign.  
 Observations are compared to our GEOS-Chem simulation and the standard version 13.3.4 of the model. PSS  
 for the NO/NO<sub>2</sub> ratio denotes a photochemical steady state as given by equation (4) and is computed mainly  
 from observed quantities. Observed NO/NO<sub>2</sub> ratios and PSS are computed only if both species are more than  
 2× above the limit of detection.

115



Deleted:

- Deleted: Vertical profile contributions to
- Deleted: columns that would be detected
- Deleted: a satellite instrument. The left panel
- Deleted: scales with
- Deleted: The middle panel
- Deleted: The right panel
- Deleted: the middle

**Figure 4.** Sensitivity of the tropospheric NO<sub>2</sub> column measured from space to the vertical distribution of NO<sub>2</sub>. Panel A shows the mean clear-sky scattering weights ( $w(z)$  in equation (3)) for the ensemble of observed vertical profiles over the SMA during KORUS-AQ. The scattering weights represent the altitude-dependent sensitivity of the detected slant column to NO<sub>2</sub> optical depth, which is proportional to number density. Panel B shows observed and simulated median vertical profiles of NO<sub>2</sub> number density in the SMA during KORUS-AQ. Panel C shows the fractional cumulative contribution to the NO<sub>2</sub> slant tropospheric column density (SCD;  $\Omega_s$  in equation (2)) from NO<sub>2</sub> below a given altitude in the SMA. The air mass factors (AMF; equation (3)) given inset are obtained by applying the scattering weights from the left panel to the shape factors from panel B and including a mean geometric AMF<sub>G</sub> of 2.70. Observed NO<sub>2</sub> number densities between 5 and 7 km are inferred from NO observations and applying PSS (equation (4)). No observations were made above 7 km and GEOS-Chem values are used there instead.



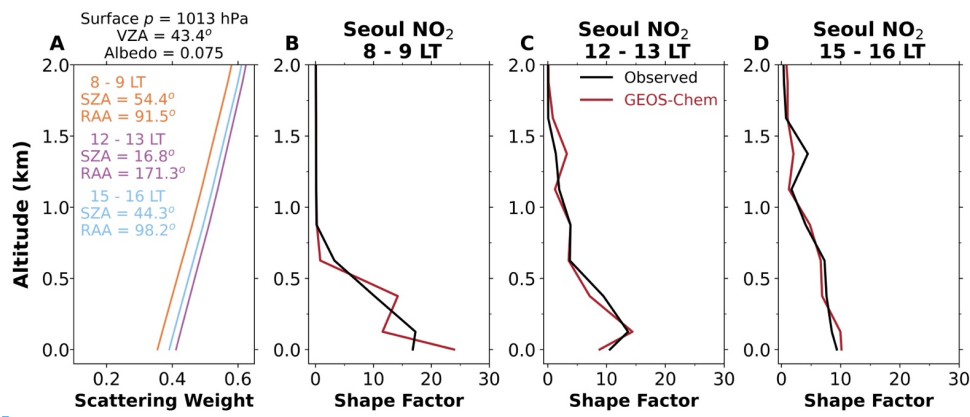


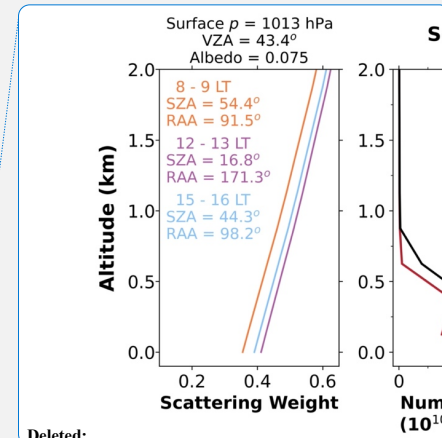
**Figure 5.** Factors controlling the diurnal variation of the air mass factor (AMF) for GEMS satellite retrieval of tropospheric NO<sub>2</sub> over Seoul. The Figure shows clear-sky scattering weights  $w(z)$  over Olympic Park in Seoul at different times of day with the GEMS viewing geometry (panel A), and vertical shape factors  $S(z)$  computed from median vertical profiles of NO<sub>2</sub> number densities at different times of the day (panels A, B, and C). Observations are from 10 KORUS-AQ flights that repeated the same flight pattern of vertical profiling under clear-sky conditions (May 4, 7, 17, 18, 30, 31; June 2, 3, 9, 10) at 8 – 9 local time (LT), 12 – 13 LT, and 15 – 16 LT. SZA and RAA are averaged over the corresponding vertical profiles. The clear-sky scattering weights are taken from the OMI TOMRAD look-up table. The shape factor is extended to the surface by using the surface air NO<sub>2</sub> concentration measured at Olympic Park station.

**Table 1.** Diurnal variation of the air mass factor (AMF) for satellite NO<sub>2</sub> retrievals<sup>1</sup>

Time of day <sup>2</sup>	SZA	RAA	AMF <sub>G</sub>	$\int_0^{z_T} w(z)S(z)dz$	AMF
8-9 LT	54.4°	91.5°	3.09	0.38 (0.39)	1.19 (1.20)
12-13 LT	16.8°	171.3°	2.42	0.46 (0.47)	1.11 (1.14)
15-16 LT	44.3°	98.2°	2.77	0.46 (0.46)	1.27 (1.28)

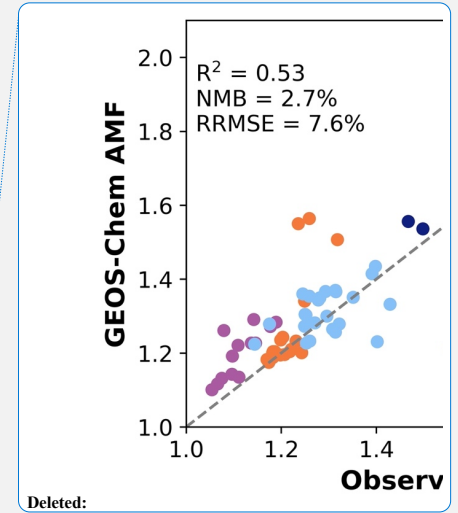
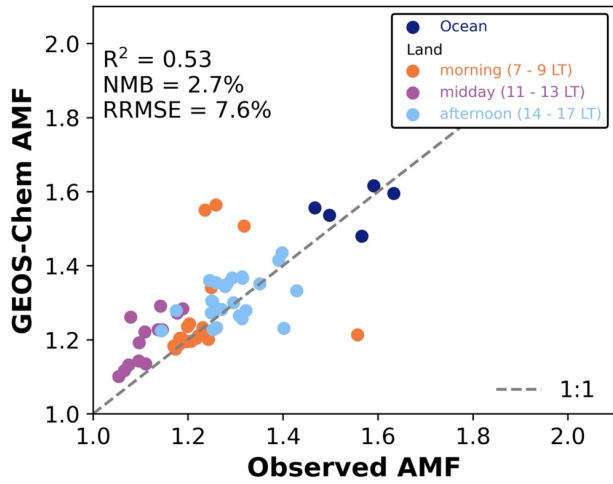
<sup>1</sup> Inferred from the median observed vertical profiles of NO<sub>2</sub> concentrations over Seoul taken during KORUS-AQ at different times of day (Figure 5). GEOS-Chem model values are in parentheses. The Table shows the AMF as computed from equation (3) and the contributions from the diurnally varying factors affecting its computation at the three different times of the day including solar zenith angle (SZA), relative azimuth angle (RAA), geometric AMF (AMF<sub>G</sub>), and scattering correction factor ( $\int_0^{z_T} w(z)S(z)dz$ ), with the scattering weights computed for clear sky. All computations use a surface albedo of 0.075, a viewing zenith angle (VZA) of 43.4°, and a surface pressure of 1013 hPa invariant with the time of day.

<sup>2</sup> Local time (LT) is Korean Standard Time (KST). Solar noon was at 1220 KST during the KORUS-AQ period.



- Deleted:
- Deleted: Clear
- Deleted: for tropospheric NO<sub>2</sub> column retrievals
- Deleted: left) and
- Deleted: .
- Deleted: shown as a symbol is from the Teledyne T500U CAPS analyzer located
- Formatted: Font: Bold

- Deleted:  $\int_0^{z_T} w(z)S(z)dz$
- Deleted: the



Deleted:

Deleted: in

Deleted: Coefficient

Deleted:

**Figure 6.** Variability of the air mass factor (AMF) for tropospheric NO<sub>2</sub> VCD retrievals from satellite as seen in 63 individual KORUS-AQ vertical profiles. The Figure compares GEOS-Chem and observed AMF calculated from equation (3). The coefficient of determination ( $R^2$ ), normalized mean bias (NMB), and relative root-mean-square error (RRMSE) are given inset. The 1:1 line is shown as dashed.